EPHA2-Ephrin-B1 *cis*-interaction supports self-renewal ability leading to recurrence of oral cancer

Reshma Raj R[1,2], Nandini Datta[1], Soumya Krishnan U[1], Geetha Shanmugam[1], Jiss Maria Louis[1], Ravichandran Damodaran Jeyaram[1], Keshava K Datta[3], Harsha Gowda[3], Meghna Sarkar[1], Madhumathy G Nair[4], Jyothy S Prabhu[4], Hafsa Shabeer[4], Balagopal P G[5, 6], Thameem A[5], Alan Jose[5], Vishnu Sunil Jaikumar[7] and Tessy Thomas Maliekal[1, 2]*

[1]Cancer Research, BRIC-Rajiv Gandhi Centre for Biotechnology, Thiruvananthapuram, Kerala, India

[2] Regional Centre for Biotechnology, Faridabad, Haryana, India

[3]Institute of Bioinformatics, Bangalore, Karnataka, India

[4]Division of Molecular Medicine, St. John's Research Institute, St John's National Academy of Health Sciences, Bangalore, India

[5]Cochin Cancer Research Centre, Cochin, Kerala, India

[6] Surgical Oncology, Regional Cancer Centre, Thiruvananthapuram, Kerala, India

[7]Animal Research Facility, BRIC-Rajiv Gandhi Centre for Biotechnology, Thiruvananthapuram, Kerala, India

* Corresponding author

E-mail: tessy@rgcb.res.in

ABSTRACT

Eph-Ephrin pathway that drives a bidirectional signaling regulates a plethora of biological activities with its varied level of complexity. While the canonical *trans*-interaction of the ligand and receptor on neighboring cells initiates forward signaling that brings about biological activities, their *cis*-interaction on the same cell attenuates the forward signaling, modulating the biological effects. Yet, non-canonical *cis*-interactions with heterotypic surface proteins and kinases regulate certain biological effects. In cancer, the canonical signaling is believed to be tumor suppressive, while the ligand-independent non-canonical signaling drives tumor progression and poor prognosis. Self-renewal ability of cancer cells is a major underlying cause of recurrence and poor prognosis of cancer. Using SILAC-based proteomics, we identified Ephrin-B1 signaling as a crucial regulator of oral cancer self-renewal. Though Ephrin-B1 is known to regulate normal stem cells, its role in cancer remains underexplored. Our biochemical analyses show that Ephrin-B1 binds to a nonconventional receptor EPHA2, which is known to regulate cancer stem cells (CSCs), though the mechanism is less explored. Contrary to the belief that the *cis*-interaction of receptors and ligands is a means to block functional signaling, our immunoprecipitation, FRET facilitated photoswitching analysis, proximity ligation assay, and *in vitro* kinase assay provide evidence for the Ephrin-B1-EPHA2 *cis*-interaction leading to the phosphorylation of EphrinB1 at Y324/329 and Y317. Extreme limiting dilution assay *in vitro* and *in vivo* confirmed that this *cis*-interaction promotes CSC enrichment. Substantiating our *in vitro* results, mouse orthotopic models showed that Ephrin-B1/EPHA2 interaction regulates prognosis. The clinical relevance of the finding was validated using a TCGA data set and immunohistochemical analysis of tissue microarray using

50 samples from oral cancer patients with recurrence in comparison to patients, who showed disease-
51 free survival. Given that Ephrin-B interacts with EphB for normal stem cell homeostasis, this
52 unconventional EPHA2/Ephrin-B1 *cis*-interaction, specifically manifested in CSC niches, might
53 serve as an attractive target for therapy, warranting further validation.

54 Introduction

55 Eph/Ephrin signaling is a bidirectional signaling, which is mediated through membrane-
56 bound Eph receptors and Ephrin ligands. Eph receptors are tyrosine kinases, which are classified
57 into A or B based on the similarity in the sequence. Humans have nine EphA receptors, five EphB
58 receptors, five Ephrin-A ligands with glycosylphosphatidylinositol (GPI) linkage, and three
59 Ephrin-B ligands with a transmembrane region. Eph/Ephrin signaling contributes to varied
60 context-dependent functions *via* a diverse range of receptor-ligand combinations, bidirectional or
61 unidirectional signaling, and Ephrin-independent non-canonical signaling of Eph receptors or Eph-
62 independent signaling of Ephrin ligands (1). During development, it is known to regulate axon
63 growth (2), tissue patterning (3), tissue boundary formation (4), migration of stem cells (5, 6), and
64 stem cell maintenance (7-10). Complementary to these developmental processes, several
65 tumorigenic properties like, proliferation, apoptosis, angiogenesis, metastasis, and immune
66 modulation, are also regulated by the Eph/Ephrin pathway (1). Thus, it is evident that unraveling
67 the complexity of this evolutionarily conserved pathway is critical for understanding different
68 biological processes.

69 In a typical bidirectional signaling, when the receptor molecule of one cell interacts with
70 the ligand molecule on a neighboring cell, i.e., a *trans* interaction, it leads to signaling events in
71 the receptor-bearing cell (forward signaling) and the ligand-bearing cell (reverse signaling). In this

72 scenario, we would expect the ligand and the receptor to be present on the neighboring cells. But
73 in many contexts, it is shown that cells co-express the ligands and the receptors, allowing the
74 possibility of a *cis*-interaction, i.e., interaction within the same cell. Using an overexpression
75 system, Yin *et al* have shown that the *cis*-interaction of EphA/Ephrin-A does not lead to signaling,
76 but it competes with the *trans* signaling, reducing the tyrosine phosphorylation of the receptor (11).
77 When the role of *cis* or *trans*-interactions of co-expressed Eph receptors and Ephrin ligands in
78 axonal guidance was tested, it was observed that the majority of the ligands and receptors of the
79 same cell segregate to different growth cones, minimizing the chance of *cis*-interaction (12).
80 Eventually, several other studies showed that the balance between *cis* and *trans* modes of ligand-
81 receptor interaction is key to the diversity of axon guidance signaling responses (13). The same
82 notion that *cis*-interaction is a means of regulating the *trans*-interaction, is shown in cancer cells
83 also. One of the reports from Pasquale's group has shown that the *cis*-interaction of EphA3 with
84 Ephrin-A3 or Ephrin-B2 is a means of regulation of EphA3 forward signaling in lung cancer.
85 Further, they have shown that one of the reported EphA3 mutations in lung cancer patients
86 enhances its *cis*-interaction to suppress the tumor suppressive effects of EphA3 signaling (14).
87 Apart from the *cis* interaction between its own family members, these ligands and receptors can
88 have heterotypic *cis*-interactions with other signaling molecules like epidermal growth factor
89 receptor (EGFR), fibroblast growth factor receptor (FGFR), Dishevelled2 (Dvl2), etc., to modulate
90 several physiological functions, which is extensively reviewed elsewhere (15). Taken together, the
91 receptors of this family can have canonical ligand-dependent activity as well as non-canonical
92 ligand-independent activity. Thus, it is evident that the outcome of Eph-Ephrin signaling depends
93 on the type of ligands and receptors, mode of interaction, and the type of heterotypic interactions.
94 Given the complexity of the system, the downstream pathway in each of these contexts is not

95 resolved. However, phosphorylations of some residues of the receptors and ligands are reported.
96 Yet, there are considerable lacunae in our understanding of how the phosphorylations of the
97 receptors and ligands lead to the specific effect. With its different layers of intricacy, this signaling
98 can tightly regulate developmental processes as well as cancer.

99 Several members of the Eph-Ephrin family are shown to be involved in regulating various
100 aspects of malignancy. As the field evolved, there is contradicting evidence suggesting the tumor
101 suppressive as well as tumor promoting role of this signaling (16). In general, it is accepted that
102 the canonical forward signaling exerts tumor suppression, while the ligand-independent-non-
103 canonical signaling promotes tumor progression (1). Although deregulations of several of the
104 family members are reported in a wide range of cancers, some of the molecules that emerge as
105 therapeutic targets are EPHA2 and EPHB2 (17-21). These receptors regulate cell proliferation,
106 invasion, metastasis, immune modulation, and cancer stem cell (CSC) properties. EPHB2 has been
107 shown to exert immunomodulation in the tumor microenvironment, and it regulates angiogenesis
108 (16). On the other hand, EPHA2 regulates CSCs along with other cancer properties. It is shown
109 to regulate CSCs of glioblastoma (22), non-small cell lung carcinoma (23), nasopharyngeal
110 carcinoma (24) and oral squamous cell carcinoma (OSCC) (25). The majority of the reports of
111 EPHA2 regulating CSCs show the ligand-independent phosphorylation on S897 to be a critical
112 regulator of the property (24, 26, 27). Another recent report has shown that EPHA2 leads to the
113 transcriptional activation of KLF4 through ERK activation (25). Even though the role of EPHA2
114 receptor in CSCs is well established, the mode of activation of EPHA2 or the ligand molecule that
115 interacts with it in CSCs, leading to these biological effects, is not extensively studied.

116 Ephrin-B1 is a ligand typically shown to bind with EphB1 or EphB2 receptor, and is well-
117 explored in the context of stem cells. Ephrin-B1-mediated EphB signaling is shown to be important
118 for the proliferation of dental pulp stem cells, and tissue repair (28, 29). Similarly, the neural
119 progenitor compartment is also regulated by this signaling (30). The role of this signaling is
120 extensively studied in mouse intestinal crypts, where the reverse gradient of EphB2/B3 and
121 Ephrin-B1 expression and signaling thereby regulates the stem cell compartment position,
122 proliferation, and differentiation (7). In spite of its well-established role in normal stem cell
123 regulation, it's contribution to cancer stem cells (CSCs) and cancer is poorly explored. However,
124 a correlative analysis has shown that Ephrin-B1 is a marker for the aggressiveness of bladder
125 cancer (31). Recently, we have reported that ablation of TUBB4B diminishes the self-renewal
126 ability of oral CSCs *in vitro*, by reducing the surface localization of Ephrin-B1, implicating its
127 role in oral cancer (32).

128 The current study was initiated with the investigation of the signaling pathways, their
129 ligands and receptors, regulating self-renewal of oral cancer cells. Since our results pointed out the
130 importance of Ephrin-B1 and the signaling mediated by this ligand, we explored the role of this
131 signaling in regulating the self-renewal ability of oral cancer cells, which leads to recurrence and
132 poor prognosis. Here, we present evidence for the interaction of Ephrin-B1 with EPHA2 in the
133 same cancer cells, leading to the phosphorylations of Ephrin-B1. Further, we explored the
134 possibility of this Ephrin-B1-EPHA2 interaction in the regulation of oral cancer prognosis using
135 mouse models and OSCC primary samples.

136

Results

Eph/Ephrin signaling is regulated in parallel to the enrichment of self-renewing cancer cells in oral cancer

Since self-renewing cancer cells are the culprits of cancer properties like tumor initiation, metastasis, and recurrence, we explored the pathways regulating self-renewal ability in oral cancer cells. The surface proteins, usually the receptors and ligands of different pathways, critically regulate the properties of cancer cells. Sphere culture is an established way of enriching the self-renewing population, which we confirmed with sustained sphere formation efficiency up to three passages, as well as increased soft agar colony formation, increased expression of stem cell markers like *ALDH1A1*, *BMI1, KLF4, NANOG,* and *OCT4A* in sphere culture compared to monolayer cells (S1A-S1E Fig). To identify the surface proteins and pathways of self-renewal in oral cancer, we performed a proteomic analysis of the surface proteins and a phosphoproteomic analysis, using sphere culture in comparison to monolayer cells after SILAC labelling (S2A-S2B Fig). We identified 148 membrane proteins specifically enriched in sphere culture (Fig 1A, S1 Table). Up-regulation of some of the surface proteins obtained from the analysis was confirmed using western blotting of the membrane preparation (Fig 1B-1C). The surface localizations of a few molecules (TUBB, TUBA1C, TUBB2A, DSG3, TUBB4B, EFNB1) were confirmed using immunofluorescence and FACS analysis (S3A Fig, Fig 1D-1E). One of the molecules found to be enriched in spheres was Ephrin-B1 (EFNB1), which is a membrane-bound ligand involved in Eph/Ephrin signaling.

Fig 1. Eph/Ephrin signaling is regulated in parallel to the enrichment of self-renewing cancer cells in oral cancer.

(A) SILAC-labelled HSC-4 oral cancer cells were grown in monolayer and sphere culture for 6 days (3D-spheres). Then we did membrane preparation followed by a SILAC based proteomic analysis using an LTQ–OrbitrapVelos ETD mass spectrometer. The Venn diagram shows the number of surface proteins enriched in spheres (148), monolayer (119), and common in both (285). (B) Some of the molecules obtained from proteomic analysis were confirmed in western blotting using lysates of 6-Day-old 3D-spheres (Sph) and monolayer (ML) of HSC-4 cells. (C) For ML and Sph, we normalized the expression with β-Actin. Then the fold change was calculated by dividing the relative expression in sphere by monolayer, and was plotted as mean ± SD values from 3 biological replicates. (D-E) HSC-4 Cells were grown in monolayer and sphere conditions for 3 days, and were used for FACS analysis to check surface expression of some of the molecules under non-permeabilizing condition. The percentage of cells showing surface expression of the indicated molecules in monolayer and spheres was plotted as mean ± SD values from 3 replicates. (F) As explained before, SILAC-labelled HSC-4 oral cancer cells grown as described earlier were used for phosphoproteomic analysis after enrichment of phosphopeptides using TiO_2 beads. The pathways differentially regulated in spheres in the two independent experiments are shown in the Venn diagram. We identified 110 unique pathways differentially regulated in spheres. (G) Among the 110 unique pathways identified, the top 20 pathways involved in self-renewal are represented in the Pie chart. (H) HSC-4 cells were grown as monolayer or sphere for 3 days, and were used for FACS analysis for surface expression of the indicated molecules under non-permeabilizing condition. The percentage of cells showing surface expression of the indicated molecules in monolayer and spheres was plotted as mean ± SD values from 3 replicates. (I) Western blot analysis of the whole cell lysates of 3-Day-old Sph or ML of HSC-4 cells. (J) Data plotted as described before. Statistical analysis was done by an unpaired-two-tailed students t-test. *, **, ***, **** represents $p<0.05$, $p<0.01$, $p<0.001$ and $p<0.0001$, respectively.

Further, to identify critical pathways, we did two independent phosphoproteomic analyses using oral cancer cells, HSC-4. The peptides and proteins identified in replicates 1 and 2 are given in S2-S4 Tables. Our duplicate analysis identified 110 unique pathways differentially regulated in spheres compared to monolayer (Fig 1F, S5 Table). From the 110 pathways, we selected 20 pathways that are shown to be linked to self-renewal either in normal or cancer contexts, are given in S6 Table and Fig 1G. Phosphorylations of some of the molecules were confirmed using western blotting (S3B Fig).

Supporting the observation of surface enrichment of Ephrin-B1 in our surface proteomic analysis, we observed that Eph/Ephrin signaling is one of the signaling pathways differentially

195 regulated in the sphere condition. Out of the 17 molecules involved in this pathway that were
196 differentially phosphorylated upon sphere condition, the ligands and receptors involved were
197 EPHA2, EPHB2, and Ephrin-B1 (S7 Table). While the ligand Ephrin-B1 and receptor EPHA2
198 showed hyperphosphorylation, EPHB2 exhibited hypophosphorylation upon sphere formation (S7
199 Table, S3C Fig). The results suggested that self-renewal enrichment is positively correlated to
200 Ephrin-B1 and EPHA2, whereas it showed a negative correlation with EPHB2. A FACS analysis
201 was performed to confirm the surface expression of receptors and ligands, which may lead to
202 signaling. In accordance with the phosphorylations observed, the surface expression of Ephrin-B1
203 and EPHA2 increased with a concomitant decrease in EPHB2 surface expression in the sphere
204 condition (Fig 1H, S3D Fig). To further explore the significance of this observation, we took 4 oral
205 cancer cell lines to analyze the differential expression in spheres and monolayer cells by western
206 blot. Western blots revealed that EPHA2 receptor and Ephrin-B1 ligand are enriched in spheres
207 across all the cell lines, while EPHB2 receptor showed no significant change in the total expression
208 except in HSC-4 cells, where it showed a significant reduction (Fig 1I-J). To confirm the specificity
209 of bands of EPHA2 and Ephrin-B1 in the western blot, we used Lentiviral shRNA-mediated
210 knock-down of the ligand and the receptor molecules. Consistent with the 57% reduction of
211 *EPHA2* transcript, we observed a 51% reduction of EPHA2 in the western blot for the 125kDa
212 band upon knock-down of EPHA2 (S4A-S4C Fig). Likewise, there was a comparable reduction
213 of Ephrin-B1 in the western blot for the 51kDa band when Ephrin-B1 was knocked down (33%
214 for both transcript and protein) (S4D-S4F Fig). Taken together, our results show that there is an
215 increased surface expression of the ligand Ephrin-B1 and the receptor EPHA2 upon the induction
216 of self-renewal in oral cancer cells. Thus, the chance of interaction of EphrinB1 with EPHA2 is
217 higher in spheres compared to monolayer.

Ephrin-B1 engages with EPHA2, and leads to differential phosphorylation in the self-renewal-enriched sphere condition

As our results indicated that in sphere condition, Ephrin-B1 might interact with EPHA2, we performed a co-immunoprecipitation (Co-IP) experiment to check whether the ligand binds to EPHA2 or EPHB2. As expected from the surface expression pattern, the level of Ephrin-B1 and its interaction with EPHA2 was higher in spheres compared to monolayer cells (Fig 2A). At the same time, Ephrin-B1 did not interact with EPHB2 in sphere or monolayer (Fig 2A). Then, the interaction of Ephrin-B1 ligand with EPHA2 receptor was validated using reverse Co-IP (Fig 2B).

Fig 2. Ephrin-B1 engages with EPHA2, and leads to differential phosphorylation in the self-renewal enriched sphere condition.

(A) HSC-4 cells were grown as monolayer or 3-Day-old spheres were used for the Co-IP experiments. Co-IP was performed with mouse Anti-Ephrin-B1 or mouse IgG (3µg) along with 7% input. The eluate was probed for the indicated molecules. (B) A reverse Co-IP experiment was performed with Rabbit Anti-EPHA2 or Rabbit IgG along with a bead only control, and 7% input. (C-D) western blotting in the whole cell lysate of monolayer or 3-Day-old spheres to check phosphorylation of indicated molecules. (E) For ML and Sph, we normalized the expression with the total form. Then the fold change was calculated by dividing the relative expression in sphere by monolayer, and was plotted as mean ± SD values from 3 biological replicates. (F) Western blotting in the whole cell lysate of 3-Day-old 3D-spheres to check phosphorylation of indicated molecules in single knock-down cells of EPHA2 or Ephrin-B1 alone or in a 1:1 mixture of both single knock-down cells. (G) We normalized the expression with the total form. Then the fold change was calculated by dividing the relative expression in knock-down by control, and was plotted as mean ± SD values from 3 biological replicates. (H) Western blotting in the whole cell lysate of 3-Day-old 3D-spheres to check phosphorylation of indicated molecules in HSC-4 cells overexpressed with plasmid control (Ephrin-B1 RFP), Ephrin-B1 Y324F RFP (We used plasmid containing Ephrin-B1 sequence of mouse. Y323 residue of mouse Ephrin-B1 protein corresponds to Y324 in human protein, so mentioned as Y324 throughout the manuscript), and Ephrin-B1 Y317F RFP (Y316 residue of mouse Ephrin-B1 protein corresponds to Y317 in human protein, so mentioned as Y317 throughout the manuscript). (I) We normalized the expression with the total form. Then the fold change was calculated by dividing the relative expression in the mutant by the wild type control, and was plotted as mean ± SD values from 3 biological replicates. (J) *In vitro* kinase assay was performed with EPHA2 kinase obtained from the eluate of the co-immunoprecipitation with either Anti-EPHA2, IgG or bead-only control, and a small stretch of synthesized peptides with specific tyrosine residues, as mentioned, acted as acceptor for the kinase assay. Negative control for the kinase assay lacked the kinase (IP eluate). The graph represents the

253 IP eluate dose curve from duplicate experiments. Statistical analysis was done by an unpaired-two-
254 tailed students t-test. *, **, ***, **** represents $p<0.05$, $p<0.01$, $p<0.001$ and $p<0.0001$,
255 respectively.

256 Next, to check whether the interaction of Ephrin-B1 ligand with EPHA2 receptor leads to
257 phosphorylation, we performed western blotting experiment to identify their phosphorylation, on
258 residues that are reported to be involved in biological activities (Fig 2C-2E). EPHA2 residues,
259 Serine 897 (S897), Tyrosine 772 (Y772), and Tyrosine 594 (Y594) were showing hyper-
260 phosphorylation in spheres. Similarly, Ephrin-B1 residues Y324/329 and Y317 were exhibiting
261 hyper-phosphorylation in spheres. Contrary to these hyper-phosphorylations, Y588 of EPHA2 was
262 showing reduced phosphorylation in spheres. As we expected, phosphorylation of EPHB2 at
263 Y594/604 residue was showing reduced phosphorylation in spheres, which implies that EPHB2
264 activation may not be important in spheres (Fig 2C-2E). So our results show that when there is an
265 enrichment of self-renewing population, there is an increased expression of Ephrin-B1 and
266 EPHA2, leading to increased phosphorylations of EPHA2 at S897, Y772, Y594, and Ephrin-B1 at
267 Y324/329 and Y317.

268 The increased phosphorylation we observed could be due to the EPHA2-Ephrin-B1
269 interaction, or it may be completely independent of it. To check that, we evaluated the change in
270 the phosphorylation pattern when the ligand or receptor is depleted. Here, we checked how much
271 of the receptor phosphorylation is blocked when the ligand is reduced and *vice versa*. None of the
272 phosphorylations of EPHA2 that were specifically upregulated in spheres (S897, Y594 and Y772)
273 were reduced upon Ephrin-B1 knock-down, suggesting that these phosphorylations are not
274 exclusive to Ephrin-B1 interaction. At the same time, the phosphorylations of Ephrin-B1 at
275 Y324/329 and Y317 were reduced significantly upon EPHA2 knock-down, which suggested that
276 these Ephrin-B1 phosphorylations are EPHA2-dependent (Fig 2F-2G). Since we focused on these

277 EPHA2-dependent Ephrin-B1 phosphorylations, we confirmed the authenticity of the bands by
278 different methods. As shown in the full blot, the phosphorylation that was reduced upon the knock-
279 down of EPHA2 was slightly heavier than the native form, and was around 55kDa (S5A- S5B
280 Fig). Subsequently, we performed cloning to mutate these specific tyrosine residues at 324 or 317
281 to phenylalanine in the Ephrin-B1 RFP plasmid to validate the phosphorylations (S6A- S6B Fig).
282 HSC-4 cells overexpressing these mutants were used to check the phosphorylations by western
283 blot. Ephrin-B1 Y324F and Ephrin-B1-Y317F mutants showed a significant reduction in the
284 phosphorylation of the corresponding residues (Fig 2H-2I). Additionally, EPHA2-dependent
285 Ephrin-B1 phosphorylations were confirmed using an *in vitro* kinase assay where the Ephrin-B1
286 peptides containing Y324 and Y329 or Y317 residues were used as acceptor, and the Co-
287 immunoprecipitated EPHA2 from spheres of oral cancer cells was used as the kinase. We show
288 that Ephrin-B1 peptides are phosphorylated by EPHA2 in a dose-dependent manner, which was
289 validated with IgG and Bead only control to negate non-specificity of antibody during the Co-
290 immunoprecipitation experiment. A reaction lacking IP eluate served as the negative control for
291 the kinase reaction. A peptide containing Y588/Y594, representing the autophosphorylation
292 residues of EPHA2, was used as the positive control for the experiment (Fig 2J).

293 To visualize this EPHA2/Ephrin-B1 interaction leading to phosphorylation of Ephrin-B1,
294 we exploited the proximity ligation assay (PLA). When we used EPHA2 and pEphrin-B Y324/329
295 primary antibody combinations for this assay in oral cancer sphere cells, we observed
296 EPHA2/Ephrin-B Y324/329 interaction as red PLA foci, where the majority of them were on the
297 cell membrane. While there were about 2 foci on average on cells in the test dish, the PLA dots
298 observed on the secondary antibody control and the IgG control were negligible (Fig 3A-3D). In
299 conclusion, our biochemical assays confirmed that the interaction of Ephrin-B1 with EPHA2 on

300 the cell membrane leads to the phosphorylation of Ephrin-B1 at Y324/329 and Y317, while it is
301 unclear whether it leads to the phosphorylation of any residues of EPHA2.

302 **Fig 3. Ephrin-B1 engages with EPHA2 at the cell membrane, and leads to Ephrin-B1**
303 **signaling in the self-renewal enriched sphere condition**.

304 HSC-4 cells grown as 3 Day-old spheres were used for the experiments. (A) Proximity ligation
305 Assay (PLA) performed with mouse EPHA2 and rabbit pEphrin-B1 Y324/329 antibodies. Red
306 spot indicates PLA signal. The cell membrane was marked using Wheat Germ Agglutinin (WGA)-
307 Alexa Fluor 488. The white arrows show the membrane localization of the PLA loci. (B) Zoomed-
308 in images of the rectangle shown in A. (C) PLA of secondary control (without primary antibodies)
309 and IgG control containing rabbit and mouse IgG antibodies. (D) Quantification of PLA foci per
310 cell in 4 fields of 60X images. 37, 29, and 45 cells were counted for secondary control, IgG control,
311 and the test, respectively. Statistical analysis was done by an unpaired-two-tailed students t-test.
312 **** represents $p<0.05$, $p<0.01$, $p<0.001$ and $p<0.0001$, respectively.

313 EPHA2/Ephrin-B1 interaction supports the self-renewing cancer
314 stem cell (CSC) pool in oral cancer cells

315 Since we anticipated that EPHA2/Ephrin-B1 interaction supports CSCs in oral cancer, we
316 evaluated the change in CSC pool with the depletion of the receptor EPHA2 and the ligand Ephrin-
317 B1. For this, we used a published CSC reporter, ALDH1A1-DsRed2 (32, 33). It was made by
318 cloning the ALDH1A1 promoter upstream of DsRed2 in the DsRed2N1 plasmid (Fig 4A).
319 Lentiviral shRNA-mediated knock-down was performed in the reporter cell lines (Fig 4B-C). We
320 analyzed ALDH1A1-positive population in the reporter cells with knock-down of EPHA2 or
321 Ephrin-B1 through FACS analysis. Our results showed that knocked-down cells in the sphere
322 condition had a higher reduction in ALDH1A1-positive population compared to CSC-enriched
323 monolayer (Fig 4D-G). Both EPHA2 or Ephrin-B1-depleted cells exhibited a significant reduction
324 in the ALDH1A1-positive CSC pool compared to control cells in the spheres as well as CSC-
325 enriched monolayers (Fig 4E-F). Further, we analyzed the ALDH1A1-positive population in dual
326 knock-down cells (both receptor and ligand), which showed superior reduction in ALDH1A1-

327 positive CSC pool compared to single knock-down cells (Fig 4G). It suggests that EPHA2/Ephrin-
328 B1 interaction is important for the maintenance of ALDH1A1-positive CSC pool.

329 **Fig 4. EPHA2/Ephrin-B1 interaction regulates self-renewing cancer stem cell pool in oral**
330 **cancer cells.**

331 (A) The vector construct of ALDH1A1-DsRed2 reporter. It was made by cloning the ALDH1A1
332 promoter gene upstream of DsRed2 in the DsRed2N1 plasmid. (B) HSC-4 Reporter cells were
333 made by stable selection with G418 and followed by FACS sorting of the ALDH1A1-DsRed2
334 positive cells. (B-C) Western blot to check the knock-down of the indicated molecules in HSC-4
335 ALDH1A1-DsRed2 cells, and the data represent fold change based on the control cells, after
336 normalizing with β-Actin. (D-E) FACS analysis to check ALDH1A1 population in knock-down
337 cells in 3-Day-old monolayer or spheres. (E) Data indicate the percentage of ALDH1A1-positive
338 CSC population, plotted as mean ± SD values from 4 replicates. Statistical analysis was done by
339 an unpaired-two-tailed students t-test. *, **, ***, **** represents $p<0.05$, $p<0.01$, $p<0.001$, and
340 $p<0.0001$ respectively.

341 To corroborate the results obtained by the CSC reporter cells, we performed more robust
342 self-renewal functional assays, like extreme limiting dilution assay (ELDA) (34). For that, we used
343 single knock-down of either receptor or ligand and dual knock-down of both for ELDA analysis
344 (S7A- S7B Fig). First, we did an *in vitro* serial dilution sphere formation assay to evaluate the
345 effect of the knock-down of the ligand and the receptor (Fig 5A). The depletion of EPHA2
346 significantly reduced the CSC frequency in oral cancer cells (4.5-fold reduction in RCB1015 and
347 2.5-fold reduction in HSC-4 cells (Fig 5B-5C, S7C Fig). Similarly, knock-down of Ephrin-B1
348 caused a 2.5-fold reduction in the CSC pool (Fig 5B-5C). Although we observed a significant
349 reduction in the CSC frequency, the single knock-down of either the receptor or ligand did not
350 substantially change the size of the spheres or the number of spheres formed in each dilution (Fig
351 5A, S7C-S7D Fig). Interestingly, the dual knock-down of EPHA2 and Ephrin-B1 drastically
352 reduced the CSC frequency (6-fold reduction), sphere size and number of spheres formed in each
353 dilution (Fig 5A-5C, S7D-S7E Fig). Thus, our observations show that abolishing both ligand and
354 receptor in the same cell, disrupting the EPHA2/Ephrin-B1 interaction, drastically depletes CSCs.

355 Then, to analyze whether *in vitro* studies are concordant with the *in vivo* scenario, we did an *in*
356 *vivo* serial dilution xenograft assay. Similar to *in vitro* results, the CSC-frequency was significantly
357 reduced upon depletion of EPHA2 or Ephrin-B1 (Fig 5D-5G, S8A- S8B Fig). Taken together, all
358 these results show that abrogation of EPHA2/Ephrin-B1 interaction abolishes CSCs *in vitro* and
359 *in vivo*. Furthermore, we did an *in vitro* serial dilution sphere formation assay with Y324F or
360 Y317F mutants of Ephrin-B1 to check the dependency of self-renewal on the phosphorylation of
361 these residues. The mutation of tyrosine 324 to phenylalanine of Ephrin-B1 (Ephrin-B1 Y324F)
362 caused a 1.7-fold reduction in the CSC frequency in oral cancer cells (Fig 5H-5J, S8C Fig).
363 Similarly, Thus, our results so far confirmed that the EPHA2-mediated phosphorylations of
364 Ephrin-B1 on Y324 and Y317 are critical for the self-renewal of oral cancer cells.

365

366 **Fig 5. Abrogation of EPHA2/Ephrin-B1 interaction depletes self-renewing cancer stem cell**
367 **pool in oral cancer cells.**

368 **(**A) RCB1015 cells with knock-down of EPHA2, Ephrin-B1 or both molecules were seeded at
369 different serial dilutions in Poly-HEMA-coated 96-well plate and were grown as spheres for 6
370 days. The image shows the spheres formed in the dilution of 10,000 cells/well. The scale bar
371 represented 100µm. (B) Cancer stem cell frequency calculated by ELDA (C) The graph represents
372 a log fraction plot obtained from ELDA analysis, and slope of it represents CSC frequency. (D)
373 For the serial dilution xenograft formation assay, cells were serially diluted and were injected
374 subcutaneously on the flanks of NSG mice. The first two figures in D represent the image of tumors
375 collected after 14 days from 10^6, and 10^5 dilutions respectively while tumors were collected after
376 40 days from 10^4 dilution. (E) Representative images of tumors collected after 17 days from all
377 the dilutions. (F-G) Tables show a summary of ELDA analysis, and graphs represent the log
378 fraction plot obtained from ELDA analysis. (H) 6-Day spheres formed of HSC-4 cells
379 overexpressed with Ephrin-B1 RFP or Ephrin-B1 Y324F RFP in a dilution of 1000 cells/well of
380 respective cells. (I-J) The table shows a summary of ELDA analysis, and the graph represents a
381 log fraction plot obtained from ELDA analysis. (K) 6-Day spheres formed of HSC-4 cells
382 overexpressing respective constructs as described before. (L-M) The table shows a summary of
383 ELDA analysis, and the graph represents a log fraction plot obtained from ELDA analysis.

Cis-interaction of EPHA2 and Ephrin-B1 regulates the self-renewing cancer stem cell (CSC) pool in oral cancer cells

Since Eph receptors and Ephrin ligands are reported to interact in *cis* (within the same cell) as well as *trans* (between neighboring cells), we evaluated these possbilities in our system. In our earlier assays of self-renewal, we have used dual knock-down system, where the receptor and the ligand of the same cell are depleted. So, in a dual knock-down system, both *cis* and *trans* interactions are compromised. Then we used the single knock-down cells, where both interactions are weakened. At the same time, when we mix these cells in equal proportions, they can restore the *trans* interaction because EPHA2 knock-down cells will express Ephrin-B1, and Ephrin-B1-depleted cells will have EPHA2. Mixing of the single knock-down cells failed to rescue the phosphorylation of both the residues of Ephrin-B1, implying that the interaction is a *cis*-interaction (Fig 2F). Then, to determine whether this *cis*-interaction leads to phosphorylation of Ephrin-B1 at tyrosine 324, we analyzed multiple confocal images of the PLA experiment. It showed a higher number of PLA foci indicating EPHA2/Ephrin-B1 Y324 interactions were on the cell membranes without cell contact than on the cell-cell junctions, which suggested *cis*-interaction leading to the phosphorylation of Ephrin-B1 in spheres (Fig 6A-6B).

Fig 6. EPHA2/Ephrin-B1 *cis*-interaction regulates self-renewal.
(A) Images of PLA showing the foci at isolated cell membranes without cell-cell contact (*cis,* arrow marks), or cell-cell junctions where we cannot distinguish whether it is *cis* or *trans*. (B) The distribution of PLA foci/cell from 63 cells in 4 fields of 60X images. Statistical analysis was done by an unpaired-two-tailed students t-test. **** represents $p<0.0001$. (C) Diagrammatic representation of FRET facilitated photoswitching used in our experiment. (i) mT-Sapphire-C1 was excited with 405 nm and emission collected with 480/40 nm filter. For PSmOrange-C1, the excitation was with 560 nm and emission collected with 575/30 nm filter. (ii) For photoswitching of PSmOrange-C1, a 488 nm laser was used. The far-red form of PSmOrange-C1 was excited with 639 nm, and emission was collected with 650/25 nm. (iii) When mT-Sapphire-C1 is excited with 405 nm, it emits light in the range of 500-570 nm, which induces photoswitching of PSmOrange-C1 if it is within 10 nm. The photoswitching can be confirmed with an excitation of 639 nm and

emission of 650/25 nm. (D) HSC-4 cells were transiently transfected with PSmOrange C1-EPHA2 and mT-Sapphire C1-Ephrin-B1 plasmids. Then, these cells were grown as spheres for 3 days. Then, we imaged FRET facilitated photoswitching in live cells where we performed a sequential acquisition, as Ex. 639 nm/ Em. 650/25 nm, Ex. 560 nm/ Em. 575/30 nm, Ex. 405 nm/ Em. 488/40 nm. Further, a pulse of 30 iterations of excitation of 405 nm was given. Then, the next cycle was Ex. 639 nm/ Em. 650/25 nm, Ex. 560 nm/ Em. 575/30 nm (E-F) Table represents the summary of ELDA analysis, and the graph represents a log fraction plot obtained from ELDA analysis of mixed cells containing an equal proportion of EPHA2 knock-down cells and Ephrin-B1 knock-down cells, and the slope of it represents CSC frequency.

To ascertain the *cis*-interaction of EPHA2 and Ephrin-B1 in live oral cancer cells in a self-renewing sphere condition, we performed a FRET facilitated photoswitching with PSmOrange-C1 and mT-Sapphire-C1, which are established photoswitching pairs (35-37). mT-Sapphire C1 excites at 399 nm (ranges from 390-420 nm) and emits a blue-green light at 511 nm (ranges from 500-570 nm) while PSmOrange-C1, which is initially orange (excitation-548 nm, emission-565 nm) undergoes photoswitching upon irradiation with blue-green light to a far red form (excitation-636 nm, emission-662 nm) (Fig 6C). For this experiment, we made PSmOrange-C1-EPHA2 and mT-Sapphire-C1-Ephrin-B1 clones by amplifying EPHA2 or Ephrin-B1 from corresponding plasmids, followed by restriction digestion and ligation into PSmOrange-C1 and mT-Sapphire-C1 plasmids (S9A-S9B Fig). Further, we transiently transfected them into oral cancer cells. If EPHA2 and Ephrin-B1 are in proximity of less than 10 nm, the emission wavelength of mT-sapphire causes photoswitching of PSmOrange to a far red variant.

PSmOrange C1-only control assured photoswitching property of PSmOrange and was the positive control for the experiment (S10A Fig), while the combination of empty vectors of PSmOrange-C1 and mT-Sapphire was kept as the negative control (S10B Fig). For our analysis, we selected cells co-expressing both constructs, which are not in proximity. We observed photoswitching on the membrane of the same cell co-expressing both PSmOrange-C1-EPHA2 and

439 mT-Sapphire-C1-Ephrin-B1, which confirmed the *cis*-interaction of EPHA2 and Ephrin-B1 (Fig
440 6D, S10C Fig). Next, to check whether the *cis* interaction is involved in self-renewal, we
441 performed an *in vitro* serial dilution sphere formation assay with a mix of equal proportions of
442 EPHA2 knocked-down cells and Ephrin-B1 knocked-down cells. These mixed cells exhibited a
443 2.3-fold reduction in the CSC frequency in oral cancer cells, which confirms the role of *cis*-
444 interaction in self-renewal of CSCs (Fig 6E-6F, S11 Fig). Collectively, we show that Ephrin-B1
445 ligand interacts with EPHA2 receptor in spheres in a *cis*-manner, and leads to the phosphorylations
446 of residues at Y324/329 and Y317 of Ephrin-B1 ligand, which contributes to the self-renewal
447 ability of CSCs.

448 Abrogation of EPHA2/Ephrin-B1 interaction increases the overall
449 survival in a mouse model of oral cancer

450 Since CSCs exhibiting self-renewal ability are shown to critically regulate the prognosis of
451 cancer, we evaluated the role of this signaling pathway in the overall survival using an orthotopic
452 mouse model of oral cancer. When mice injected with EPHA2 or Ephrin-B1 knocked-down cells
453 exhibited a delayed tumor progression, mice injected with dual knocked-down cells displayed a
454 drastic retardation in tumor progression (Fig 7A-7B). Then, we used Kaplan-Meier analysis to
455 study the prognosis. Though, there was a trend in the Ephrin-B1-depleted group to show improved
456 overall survival, single knock-down of either receptor or ligand was incapable of significantly
457 altering the overall survival of the mice. In contrast, mice injected with dual knocked-down cells
458 showed a significant improvement in overall survival (Fig 7C). Furthermore, the expression of
459 self-renewal molecules like SOX2 and OCT4A showed a reduction in the ligand or receptor-
460 knocked-down tumors (S12A- S12B Fig). In agreement with this, xenograft tissue sections with

knock-down of receptor or ligand (S12C- S12E Fig) showed reduced expression of ALDH1A1 (S12C, S12F Fig). To confirm the role of Ephrin-B1 phosphorylations in self-renewing CSCs *in vivo*, we used the serial sections of the orthotopic tumors for immunofluorescence. As expected, phosphorylation of Ephrin-B Y324/329 on the cell membrane was high in the regions where ALDH1A1 was high, compared to the ALDH1A1^{low} region (Fig 7D-7E). More important observation was the high co-localization of EPHA2 and phospho-Ephrin-B Y324/329 on the cell membrane of cells in the ALDH^{high} region as revealed by Pearson's correlation analysis Scatter Plot (Fig 7D) and the Pearson's correlation coefficient (Fig 7F). Our results clearly demonstrate the increased interaction of EPHA2 with Ephrin-B, thereby increasing the phosphorylation of Ephrin-B Y324/329 on the ALDH^{high} region. To summarize, the interaction of EPHA2 and Ephrin-B1 in the CSC niche supports the sustenance of CSCs, and the loss of EPHA2 and Ephrin-B1 in the same cell reduces the tumor progression and improves the prognosis by enhancing overall survival in mouse models.

Fig 7. Role EPHA2/Ephrin-B1 interaction supports ALDH1A1 population leading to poor prognosis in oral cancer mouse model.
Overall survival analysis was performed using an orthotopic floor of the mouth mice model. 0.5×10^6 cells were injected into the floor of the mouth region superficial to the mylohyoid muscle. RCB1015 shControl, shEPHA2 and shEphrin-B1 cells were injected into SCID mice, while RCB1015 shControl and shDual, cells were injected into NSG mice. (A) Representative image of mice with a tumor after 24 days. (B) We measured tumor size using a digital Vernier caliper at regular intervals and plotted tumor volume against the number of Days. Tumor volume was calculated using the formula (Height*Height*width)/2. (C) Kaplan-Meier survival analysis was performed using GraphPad Prism to check overall survival. (D) Xenograft serial sections were co-stained for ALDH1A1/Ephrin-B Y324/329 or EPHA2/Ephrin-B Y324/329. We chose two regions, one with high expression of ALDH1A1 (ALDH1A1^{high}) and the other with low expression of ALDH1A1 (ALDH1A1^{low}), and the same regions were identified on the next serial section that were stained for EPHA2/Ephrin-B Y324/329 and represented with an image of high magnification. The Scatter plots represent Pearson analysis between EPHA2 and phospho-Ephrin-B Y324/329 of ALDH1A1 high and low regions in the whole field. (E) Mean intensity of Ephrin-B Y324/329 was calculated from the cell membranes of 75 cells each from 3 fields of ALDH1A1 high and low regions. (F) ROI was drawn for cell membranes of 75 cells from 3 fields and calculated Pearson's correlation coefficient between EPHA2 and phospho-Ephrin-B Y324/329 in ALDH1A1 high and

low regions. Statistical analysis was done by an unpaired-two-tailed students t-test. *, **, **** represents $p<0.05$, $p<0.01$, $p<0.001$ and $p<0.0001$, respectively.

EPHA2/Ephrin-B1 interaction critically regulates the prognosis of oral cancer

Data from our mouse model, demonstrating the role of EPHA2/Ephrin-B1 interaction in the regulation of overall survival, prompted us to explore the role of this signaling in overall survival of oral cancer patients. First, we checked whether there were any differences in the expression of the ligand and the receptors identified in our study, using a TCGA dataset of oral cancers compared to the normal tissues. The transcript levels of Ephrin-B1 (*EFNB1*) and EPHB2 (*EPHB2*) were significantly upregulated in the malignant tissues compared to their normal counterparts. Though there was a trend of upregulation, the levels of EPHA2 (*EPHA2*) did not significantly change in the two conditions (S13A Fig). Yet, when we analyzed the correlation of Ephrin-B1 with the receptors using a hierarchical clustering heat map analysis of TCGA data, the correlation with *EPHA2* was higher than with *EPHB2* receptor (S13B-S13C Fig). Then, we evaluated the protein expression of EPHA2, EPHB2, and Ephrin-B1 in relation to ALDH1A1 on the primary oral cancer tissue sections to check the dependency of this signaling on CSCs. An immunohistochemical analysis of oral cancer samples co-stained with these four molecules revealed that while the expression of EPHA2 receptor and Ephrin-B1 ligand is confined to certain clusters, the expression of EPHB2 is uniform throughout the section (Fig 8A). More specifically, some regions of the tissue sections had high expression of both EPHA2 and Ephrin-B1, which showed a better co-localization than the Ephrin-B1-EPHB2 co-localization, as revealed by Pearson's correlation analysis (Fig 8B). Hence, in accordance with our *in vitro* cell line data, the primary oral cancer sample data also suggest EPHA2-Ephrin-B1 co-localization leads to signaling

within the region positive for ALDH1A1, defining the CSC niches of the tumors. The expressions of both Ephrin-B1 and EPHA2 were observed in the same cell, suggesting the *cis*-interaction, which we deduced from our biochemical analysis. Here, we observed that the ALDH1A1 population is restricted to the region where EPHA2-Ephrin-B1 co-localization is seen (Fig 8A), supporting the notion that the interaction of EPHA2 and Ephrin-B1 in the same cell enriches self-renewing CSCs in oral cancer.

Fig 8. EPHA2/Ephrin-B1 interaction in oral cancer tissues.

(A) OSCC patient samples were co-stained for the indicated molecules using tagged primary antibodies, EPHB2-Alexa 405, EPHA2-Alexa 488, EphrinB1-Alexa 680, and ALDH1A1-Alexa 568. (B) From multiple images at 40X, we chose 12 ROI to check the co-localization using Pearson's correlation analysis. **, ***, **** represents $p<0.01$, $p<0.001$ and $p<0.0001$, respectively.

Next, we tested whether the expression of *EFNB1* and *EPHA2* correlates with overall survival. Although patients with the high expression of either the ligand or receptor did not show any difference in the prognosis, the high expression of both the receptor and ligand exhibited poor overall survival compared to the group showing the low expression of both (Fig 9A-9C). Since the prognosis of oral cancer is dependent on the recurrence of the disease, we also studied that aspect. We segregated oral cancer patients into the recurrent and disease-free category, with a cut-off of 15 months' disease-free survival. Then a tissue microarray immunohistochemical (IHC) analysis was performed on recurrent and disease-free OSCC samples using EPHA2 and Ephrin-B1 antibodies (Fig 9D). Irrespective of the survival status, the expression of the receptor was high in all tumor tissues. On the other hand, Ephrin-B1 expression was limited to the outer layers of tumor bundles rather than the core of the bundle. Then, tumor bundles in the samples were scored based on the co-expression of high EPHA2 ($EPHA2^{Hi}$) with concomitant Ephrin-B1 positivity. Then, the

percentage of tumor bundles with co-localization of EPHA2^{Hi} and Ephrin-B1^{+} in each sample was calculated. The co-expression of the ligand Ephrin-B1 and the receptor EPHA2 offers a chance for their interaction to modulate signaling. The recurrent group showed a higher percentage of tumor bundles (>30%) with co-localization of EPHA2^{Hi} and Ephrin-B1^{+} than the disease-free group (Fig 9E).

Fig 9. Role of EPHA2/Ephrin-B1 interaction in the prognosis of oral cancer patients.

(A-C) A TCGA data set was used to study overall survival in HNSCC patients. Patients were categorized according to the level of expression of EPHA2 and Ephrin-B1, as described under Materials and Methods. The table represents the summary of statistics (D) A tissue microarray IHC was performed on serial sections of recurrent or disease-free samples Images from three patients from each group are shown (E) Then, tumor bundles in the samples were scored based on the co-localization of high expression of EPHA2 (EPHA2^{Hi}) and Ephrin-B1 in the sample. Then, the percentage of tumor bundles with co-expression of EPHA2^{Hi} and Ephrin-B1^{+} in each sample was calculated. (F) The patients were segregated into two groups, using a cut-off of 30% of tumor bundles with co-expression of EPHA2^{Hi} and Ephrin-B1. A Kaplan-Meier survival graph for disease-free survival was plotted between those two groups.

Kaplan-Meier survival analysis showed that patients with a lower extent of co-expression of Ephrin-B1^{+} and EPHA2^{Hi} (<30% of the tumor bundles) show better disease-free survival compared to patients with a higher extent of their co-expression (>30%) (Fig 9F). Thus, our IHC analysis of the tissue microarray reinforced our hypothesis that the interaction of Ephrin-B1 with EPHA2, in *cis*, critically regulates recurrence of oral cancer.

Discussion

Recurrence is a major driving factor for poor prognosis in many cancers, including lung, breast, bladder, and oral cancer (38-42). Among these cancers, oral cancer is a major burden in Asian countries, especially in India. Recurrence occurring as loco-regional or distant metastasis leads to the death of one out of two oral cancer patients (42, 43). The recurrence depends more on

567 the self-renewal property of cancer cells than on the stage and grade of the cancer (44, 45).
568 Therefore, it is essential to target these self-renewing cancer stem cells (CSCs) for which we need
569 to identify surface proteins and pathways that regulate them. In self-renewal-enriched spheres, we
570 identified the enrichment of the surface expression of Ephrin-B1 ligand, which is a mediator of
571 Eph-Ephrin signaling. Moreover, a phosphoproteomic analysis identified Eph-Ephrin signaling as
572 one of the differentially regulated pathways in spheres. The phosphorylation pattern and
573 enrichment of the ligand and receptors in the sphere condition suggested the possibility of Ephrin-
574 B1/EPHA2 signaling, supporting CSCs (Fig 1). Though cross-signaling is possible for Eph-Ephrin
575 signaling, the majority of studies have shown that EPHA2 interacts with Ephrin-A, while Ephrin-
576 B1 interacts with EPHB. In this context, if we find that EPHA2 interacts with Ephrin-B1 to support
577 CSCs, it will be a novel interaction that can be targeted for eradicating CSCs.

578 Though Ephrin-B1 is established to regulate normal stem cells, its role in CSCs is less
579 investigated except for the first report from our lab, which showed that the regulation of surface
580 expression of Ephrin-B1 by TUBB4B is essential for the support of CSCs in oral cancer (32).
581 Ephrin-B1, however, is reported to be overexpressed in many cancers, including oral cancer (32,
582 46, 47). Also, the over-expression is correlated to angiogenesis, aggressiveness of tumor, and
583 recurrence, though the molecular mechanism by which it regulates cancer progression is elusive
584 (46). Even though the EPHB2 receptor is reported as the regular binding partner for Ephrin-B1 in
585 different contexts, as stem cell-homeostasis of intestinal crypt as well as cancer. During cancer
586 progression, EPHB2/Ephrin-B1 signaling regulates invasion, metastasis, and immunomodulation
587 (7, 18, 48). But whether the same receptor molecule interacts with Ephrin-B1 in the CSC context
588 is unknown. Since our findings suggested that Ephrin-B1 and its signaling are crucial in regulating

589 the self-renewal of cancer cells, it is essential to identify the modulators of Ephrin-B1 to regulate
590 self-renewal.

591 The receptor molecules obtained from our phospho-proteomic analysis, EPHB2 and
592 EPHA2, are reported to be overexpressed in HNSCC and oral cancer, respectively (25, 49). Higher
593 expression of these receptor molecules in cancer patients leads to poor prognosis in patients,
594 implying that they have a role in the progression of cancer (25, 50). Consistent with this, our data
595 revealed that *EPHB2* transcripts and its protein are high in oral cancer, suggesting its role in the
596 regulation of malignant properties (S12A Fig, Fig 8A). Although our results did not support the
597 role of EPHB2 in the self-renewal in oral cancer, it is reported to enrich CSCs to impart sorafenib
598 resistance in hepatocellular carcinoma, by the up-regulation of the WNT-β-catenin pathway (51).
599 Despite that, its expression is a predictive marker for relapse-free survival in colorectal cancer,
600 gastric cancer, and breast cancer, disproving its role as a universal positive regulator of CSCs and
601 recurrence in all malignancies (52-54). Even if EPHB2 does not regulate the self-renewal property
602 of CSCs, the signaling mediated by the receptor might have critical roles in other malignant
603 properties. The EPHB-Ephrin-B interaction is reported to induce fibroblast remodeling to generate
604 cancer-associated fibroblasts (CAFs), and increase invasion and metastasis (55).

605 As we consider the second receptor EPHA2, it is demonstrated to regulate CSCs of many
606 cancers, including oral cancer, which aligns with our findings (22, 23, 25). Additionally, our study
607 proposes the role of EPHA2 receptor in regulating recurrence, as we observed the co-expression
608 of EPHA2 receptor and Ephrin-B1 ligand correlates with recurrence in oral cancer patients (Fig
609 9D-9F, S13A Fig). Since we observed that there is enhanced surface expression of Ephrin-B1
610 ligand and EPHA2 receptor when there is an induction of self-renewal (Fig 1I-1J), we investigated

611 whether they interact to initiate signaling. Our co-immunoprecipitation experiments indicated that
612 the co-expression of EPHA2 and Ephrin-B1 in the self-renewal-enriched sphere condition results
613 in their interaction (Fig 2A-2B). Our western blot analyses showed that in the self-renewal-
614 enriched condition, there is differential regulation of phosphorylation in the ligand as well as
615 receptors (Fig 2C-2E). We detected a variation in receptor phosphorylations upon self-renewal
616 enrichment. Phosphorylations of EphB receptor at Y594/604, and Y588 of EPHA2 were reduced,
617 while S897, Y772, and Y594 residues of EPHA2 receptor were increased. When we used the single
618 knock-down cells to evaluate the interdependence of Ephrin-B1 and EPHA2 for the differentially
619 regulated phosphorylations, only the ligand phosphorylations were dependent on EPHA2, whereas
620 receptor phosphorylations were independent of Ephrin-B1 interaction (Fig 2F-2G). The specificity
621 of the residues of Ephrin-B1 phosphorylations was confirmed when we observed a reduction of
622 phosphorylations of Y324/329 and Y317 upon overexpression of Y324F and Y317F mutants (Fig
623 2H-2I). Further, *in vitro* kinase assay substantiated that EPHA2 phosphorylates Ephrin-B1 residues
624 Y324/329 and Y317 by (Fig 2J). Moreover, we could visualize the interaction of EPHA2 leading
625 to the phosphorylation of Ephrin-B324/329 on the cell membrane of oral cancer cells under sphere
626 culture using proximity ligation assay (PLA). The specific foci observed on the cell membrane
627 reinforced our argument that EPHA2-Ephrin-B1 interactions could lead to the phosphorylation of
628 Ephrin-B1 residues (Fig 3).

629 The functional consequences of the phosphorylations of ligands and receptors in the
630 Eph/Ephrin family are not studied extensively. Yet, ligand-mediated phosphorylations of the
631 receptors for the forward signaling are reported in different contexts. In many instances, the
632 receptor phosphorylations are mediated by heterotypic receptors and other kinases. One such
633 phosphorylation is of EPHA2 S897, a critical event regulating CSCs (24). This phosphorylation is

634 shown to be ligand-independent, regulated by kinases other than EPH receptors, like Protein
635 Kinase B (AKT), Protein Kinase C (PKC), and Ribosomal S6 kinase (RSK) (56-58). Another
636 example of ligand-independent EPHA2 phosphorylation is at Y772, which is mediated by Focal
637 Adhesion Kinases (59). Moreover, this ligand-independent EPHA2 Y772 phosphorylation is
638 shown to promote proliferation and anchorage-independent growth (60). In accordance with these,
639 we observed increased phosphorylation of EPHA2 S897 and Y772 in spheres that show anchorage-
640 independent growth and enrichment of CSCs. Since these phosphorylations are independent of
641 Ephrin ligands, they did not change with the loss of Ephrin-B1 (Fig 2J). Further, our results indicate
642 that these heterotypic interactions of EPHA2 are independent of its *cis*-interaction with Ephrin-
643 B1.

644 Though not reported in the CSC context, the classical ligand-dependent phosphorylations
645 of EPHA2 are of Y588 and Y594, the two juxtamembrane domain residues that are reported to be
646 autophosphorylated upon Ephrin-A1 ligand binding (1). These residues interact with the kinase
647 domain in an unphosphorylated form, and this interaction is critical for the autoinhibition of the
648 kinase domain (61). To the best of our knowledge, a direct substrate of EPHA2 kinase other than
649 these two residues has not been reported. In our study, we found an increase in the phosphorylation
650 of Y594 and a concomitant decrease in Y588 in sphere cells. So, our results suggest that the two
651 autophosphorylations may not be interdependent. Crystal structure analysis has revealed that both
652 Y588 and Y594 interact with the same pocket of the kinase domain (61). Nevertheless, whether
653 these two residues are phosphorylated simultaneously, sequentially, or independently of each other
654 has not been addressed so far. Upon phosphorylation, Y588 and Y594 bind to Vav2 and Vav3
655 guanine nucleotide exchange factors, respectively, to regulate Rac-mediated activities (62). The
656 signaling events downstream of Vav3 may be synergistic or independent of Vav2 effects,

657 depending on the context (63). In the sphere condition, where EPHA2 is interacting with Ephrin-
658 B1, it leads to the phosphorylation of only Y594 of EPHA2, unlike when it interacts with Ephrin-
659 A, its well-established ligand. The difference between these interactions and the subsequent
660 phosphorylations of the receptor EPHA2 needs further evaluation. As we observed no change in
661 the non-canonical activation of EPHA2 (Y772 and S897), it appears that *cis*-interaction of EPHA2
662 with Ephrin-B1 does not affect its interaction with other kinases. While we focused on
663 phosphoforms with commercially available antibodies, we acknowledge the possibility of
664 phosphorylation occurring at other EPHA2 residues, which we haven't explored. In addition, the
665 increased phosphorylation of EPHA2 may play a role in regulating CSCs, though this does not
666 seem to rely on Ephrin-B1 interaction.

667 There are considerable reports arguing that the ligand-mediated receptor phosphorylations
668 lead to forward signaling. However, reports of receptor-induced modifications of ligands leading
669 to reverse signaling, are rare. Even if the functional significance of the Ephrin-B1 ligand
670 phosphorylations, both Y324/329 and Y317, is not known, they are identified as phosphorylations
671 induced by soluble EphB2 (64). The available reports do not reveal the interaction of Ephrin-B1
672 with receptors other than EphB. Since our focus was on Ephrin-B1- EPHA2 interaction, we further
673 explored the signaling initiated by it. It is well established that Eph receptors and Ephrin ligands
674 can interact in *trans* or *cis*, where conventionally the *trans*-interaction leads to signaling events,
675 and the *cis*-interaction blocks the *trans*-interaction (14, 65). Interestingly, there is a very recent
676 article that shows Ephrin-A1 fuels cervical cancer progression by its *cis*-interaction with EPHA2
677 (66). In agreement with this, here we show that EPHA2-Ephrin-B1 *cis*-interaction leads to
678 signaling events. The pattern of PLA foci, especially the presence of foci on cell membranes where
679 there is no cell-cell contact, suggested that the interaction could be a *cis*-interaction (Fig 6A-6B).

680 This prompted us to explore the possibility in detail. As the co-culture of single knock-down of
681 ligand or receptor retains the *trans* interaction while blocking the *cis* interaction, we performed
682 our western blot analysis of the phosphoforms in that condition. Here, we showed that the *trans*
683 interaction of the ligand and the receptor does not compensate for the loss of phosphorylation,
684 suggesting that the *cis*-interaction of Ephrin-B1 with EPHA2 leads to Ephrin-B1 phosphorylation
685 (Fig 2H-2I). To substantiate this novel finding we performed a live FRET facilitated
686 photoswitching using PSmOrange-C1-EPHA2 and mT-Sapphire-C1-Ephrin-B1. We observed
687 photoswitching in cells co-expressing both constructs, confirming the *cis*-interaction of the ligand
688 and receptor (Fig 6C).

689 So far, our results demonstrate that in a self-renewal enriching condition, there is enhanced
690 co-expression of EPHA2 and Ephrin-B1, increasing their interaction and phosphorylation.
691 Although the ligands and receptors may interact in *cis* or *trans*, the interaction of Ephrin-B1 with
692 EPHA2 in *cis* is a critical signaling event in the sphere condition. Next, we analyzed the functional
693 significance of this novel EPHA2-Ephrin-B1 interaction and signaling. As our results indicated
694 that the EphrinB1-EPHA2 interaction is important for self-renewal, we explored the relevance of
695 this interaction in CSCs and recurrence. Our FACS analysis with ALDH1A1-DsRed2 CSC reporter
696 cells showed the dependence of CSCs on EPHA2-Ephrin-B1 signaling. Our results showed a
697 pronounced reduction in CSC frequency in dual knock-down cells compared to single knock-down
698 cells, where the ligand-receptor interaction is blocked (Fig 4). Extreme limiting dilution assay
699 (ELDA), a functional assay to evaluate the CSC frequency, corroborated the results of our reporter
700 assay, both *in vitro* and *in vivo* (Fig 5, S7 Fig, S8A-B Fig). ELDA, using a mix of single knock-
701 downs to restore *trans*-interaction, showed that reinstating the *trans*-interaction did not recover the
702 loss of CSC pool (S10D Fig). Thus, it is evident that the *cis*-interaction is the major mode of CSC

703 regulation. Next, to examine whether this regulation of CSCs by EPHA2-Ephrin-B1 *cis*-
704 interaction decides the prognosis, we checked overall survival using orthotopic floor of the mouth
705 mouse model (Fig 7A-7C). The drastic reduction we observed in the dual knock-down cells was
706 indeed due to the depletion of CSCs as revealed by the depletion of ALDH1A1 and other self-
707 renewal markers (S11 Fig). Further, analysis of the xenograft sections showed that the interaction
708 of EPHA2 with phosphorylated Ephrin-B is significantly enhanced on cell membranes of CSC
709 niches compared to other regions, supporting our claim that EPHA2-Ephrin-B1 *cis*-interaction is
710 crucial to enrich CSCs (Fig 7D-7G). Next, we validated the clinical significance of our
711 observations using a TCGA data set of HNSCC patients. Kaplan-Meier analysis showed that the
712 patients with higher expression of both receptor and ligand had decreased overall survival time
713 compared to patients having low expression of both, underscoring the significance of this
714 interaction (Fig 9A-9C). Further, this observation was validated by IHC of the tissue microarray
715 of OSCC samples. The pattern of expression of EPHA2 and Ephrin-B1 in OSCC samples suggest
716 that the *cis*-interaction is clearly enhanced in malignant tissues of patients. More important
717 observation was the significant increase of the EPHA2-Ephrin-B1 co-expression (and thereby their
718 interaction) in patients who showed recurrence within 15 months compared to patients who
719 showed disease-free-survival (Fig 9D-9F). To conclude, in the current study, we demonstrate the
720 importance of Ephrin-B1 in the regulation of the self-renewal ability of oral cancer cells, which in
721 turn regulates the chance of recurrence of the disease.

722 Though ligand molecules are implicated in cancer progression, the underlying mechanism
723 is largely unknown. To the best of our knowledge, this is the first study revealing how Ephrin-B1
724 ligand regulates cancer progression and recurrence. The recent report (66) and our study challenge
725 the conventional belief that receptors and their *trans*-forward signaling are the primary drivers of

signaling, whereas *cis*-interactions serve only to block signaling. We argue that *cis*-interactions of ligands, even to nonconventional receptors, regulate signaling and cancer progression. Furthermore, this *cis*-interaction could be relevant to other contexts, particularly where a reverse gradient of ligands and receptors is observed, such as in stem cell niches. Given that Ephrin-B interacts with EphB for normal stem cell homeostasis, this nonconventional EPHA2/Ephrin-B1 *cis*-interaction, specifically manifested in CSC niches, might serve as an attractive target for therapy, warranting further validation.

Materials and Methods

Ethics statement

For the studies involving fresh oral cancer samples, the tumor tissues were collected after getting informed consent from the patients from the Regional Cancer Centre, Thiruvananthapuram. The protocol was approved by the Institute Human Ethical Committee of Rajiv Gandhi Centre for Biotechnology (IHEC/1/2011/04), and Regional Cancer Centre, Thiruvananthapuram (HEC/24/2011). Paraffin embedded tissue blocks for making the tissue microarray (TMA) were collected from the archives of Cochin Cancer Research Centre, Cochin, and the preparation of TMA, IHC staining, scoring and imaging were done at St. Johns Research Institute. The protocol was approved by Institute Human Ethical Committee of all the respective study centers (IEC/150/2023, IHEC/1112022_Exl11). All the animal experiments were conducted adhering to the ARRIVE guidelines, and as per the approved guidelines of the Institute Animal Ethics Committee (IAEC/874/TM/2002, IAEC/875/TM/2002 and IAEC/894/TM/2002) which is under the Committee for the Control and Supervision of Experiments on Animals (CCSEA), Govt. of

India. The recombinant DNA works were reviewed and approved by the Institutional Bio-safety Committee (71/IBSC/TTM/2022, 72/IBSC/TTM/2022).

Antibodies

The antibodies, p-Raf-1, p38 MAPK (MAPK 1/3), TUBB, TUBB2A, TUBA1C, TUBB4B, ERO1L, TUBB3, NDRG1, GAL3, FSCN, GAL1, DSG3, ALDH1A1, Ephrin-B1, EPHA2, EPHB2, mouse IgG and β-Actin were purchased from Santa Cruz Biotechnology, Inc., Dallas, Texas, USA. The other antibodies used were either from Cell Signaling Technology, Danvers, Massachusetts, USA [p-Bad, p-Akt, p-STAT3, pp38 MAPK, SOX-2, OCT4A, EPHA2, Ephrin-B1, pEPHA2 (S897), pEPHA2 (Y772), pEPHA2 (Y594), pEPHA2 (Y588), pEphrin-B (Y324/329), rabbit IgG] or (Thermo Fisher Scientific, Waltham, Massachusetts, USA [pEPHB1/2 (Y594/604), pEphrin-B1 (Y317)]. Peroxidase conjugated AffiniPure Donkey Anti Mouse, AffiniPure Donkey Anti Goat, and AffiniPure Donkey Anti-Rabbit Secondary Antibodies were purchased from Jackson ImmunoResearch Laboratories Inc., West Baltimore Pike, West Grove, PA 19390, USA. Peroxidase conjugated Veriblot for Co-IP experiments was purchased from Abcam, Cambridge, United Kingdom. We used Donkey Anti-Rabbit Alexa Fluor-568, Donkey Anti-Mouse Alexa Fluor-568, Donkey Anti-Rabbit Alexa Fluor-488, Donkey Anti-mouse Alexa Fluor-488, Donkey Anti-Rabbit Alexa Fluor-680, and Donkey Anti-mouse Alexa Fluor-680 (ThermoFisher Scientific, Waltham, Massachusetts, USA) for immunofluorescence and immunohistochemistry experiments.

Plasmids

pCLXSN-EPHA2 Flag was a gift from the laboratory of Jin Chen (Addgene plasmid # 102755) (23). FUW-ubiquitin-Ephrin-B1-SV40-RFP (biR) was a gift from Eduard Batlle

770 (Addgene plasmid # 65446) (67). pPSmOrange-C1 was a gift from Vladislav Verkhusha (Addgene
771 plasmid # 31899) (37). mT-Sapphire-C1 was a gift from Michael Davidson and Robert Campbell
772 (Addgene plasmid # 54569) (35).

773 Cell lines

774 The cell lines RCB1015, RCB1017, HSC-4, and HSC-3 were obtained from Riken Cell
775 Bank, Japan. All these cell lines were maintained in Dulbecco's Modified Eagle's Media with 10%
776 FBS. HSC-4 and HSC-3 cells with stable expression of ALDH1A1-DsRed2 were maintained in
777 20µg/mL geneticin-containing medium. Cells stably infected with LV-shRNA particles were
778 maintained in 100ng/mL puromycin-containing medium.

779 Monolayer and sphere culture

780 Sphere cells were grown in suspension using Opti-MEM (1X) (Thermo Fisher Scientific,
781 Waltham, Massachusetts, USA), reduced serum medium supplemented with 1X N-2, 20µg/ml
782 EGF and bFGF, and 1X Insulin-Transferrin-Selenium (sphere medium) on a non-adherent dish
783 (coated with 1% Poly (2-hydroxyethyl methacrylate) or polyHEMA to deplete adherence of the
784 dish). All the supplements mentioned above are purchased from Thermo Fisher Scientific,
785 Waltham, Massachusetts, USA. Monolayer culture was maintained in DMEM (Thermo Fisher
786 Scientific, Waltham, Massachusetts, USA) in the presence of 10% FBS (Thermo Fisher Scientific,
787 Waltham, Massachusetts, USA).

788 ## Soft agar colony formation assay

789 The assay was performed using both monolayer and sphere culture. 5000 cells were seeded
790 for the analysis. After 21 days, the colonies were counted at 10X magnification, and number of
791 colonies/10 fields were plotted.

792 ## RNA isolation, RT-PCR (Reverse transcription PCR) and qRT-PCR

793 We used the RNeasy mini kit (Qiagen, Hilden, Germany) for RNA isolation from the oral
794 cancer cells. Then, the isolated RNA was quantified using NanoDrop for cDNA preparation. A
795 reaction mix containing RNA (3.5 µg), 5X RT buffer (1X), DNTP (0.1mM), random hexamer
796 primer (10µM), reverse transcriptase enzyme, and RiboLock (reagents for reverse transcription
797 were purchased from ThermoFisher Scientific, Waltham, Massachusetts, USA) was used to reverse
798 transcribe total RNA to cDNA. Further, we performed PCR to check gene expression using gene-
799 specific primers and separated DNA bands using agarose gel for electrophoresis. Then, bands were
800 visualized in Gel Doc EZ imager (Bio-Rad Laboratories, Hercules, California, USA). Similarly,
801 we prepared cDNA and performed qPCR using Power SYBR™ Green PCR Master Mix
802 (ThermoFisher Scientific, Waltham, Massachusetts, USA). Primers for *EPHA2* are F: 5'-
803 TTACCGCAAGAAGGGAGACT-3', R: 5'-GACAGCGTCTGGAATTCGT-3'. Primers for
804 *EFNB1* F: 5'-GGCAAGATCCCAATGCTGTG-3', R: 5'-GTTCACAGTCTCATGCTTGCC-3',
805 Primers for *β-Actin* are F: 5'-CCTTCCTTCCTGGGCATGG-3', R: 5'-
806 CGCTCAGGAGGAGCAATGA-3'. qPCR results obtained as cycle threshold (Ct) values. The
807 gene expression of specific gene was normalized with expression of *β-Actin* followed with fold
808 change calculation using $2^{-\Delta\Delta Ct}$ method.

809 ## SILAC labeling

810 For SILAC labeling, HSC-4 monolayer cells were grown in arginine and lysine-free
811 DMEM (ThermoFisher Scientific, Waltham, Massachusetts, USA) supplemented with heavy
812 arginine and lysine ($^{13}C_6$ Arg/$^{13}C_6$Lys;+6Da and +4 Da). SILAC-labeled cells were grown as
813 monolayer cultures while HSC-4 sphere cells were maintained in sphere medium as mentioned
814 above.

815 ## Membrane preparation for LC-MS/MS analysis

816 The sample preparation and proteomic analysis were done as reported before (68). The cell
817 lysis was done in a high salt buffer (2M NaCl, 10mM HEPES, pH 7.5, 1mM EDTA, pH 8.0) using
818 a polytron tissue homogenizer. The supernatant collected after the centrifugation of the lysate at
819 250,000 g for 45 min at 4°C was discarded, and the pellet was re-suspended in 0.1 M Na2CO3,
820 pH 11.0, using a polytron homogenizer, and left on ice for 45 min. The high salt lysis and Na2CO3
821 wash were repeated an additional two times, and the pellet containing the membranous material
822 was used for LC-MS/MS analysis using hybrid LTQ–OrbitrapVelos ETD.

823 ## Cell lysis, Trypsin digestion, phosphopeptide enrichment for LC-
824 ## MS/MS analysis

825 The sample preparation was carried out as described before (69). Briefly, the monolayer
826 cells were scraped in PBS and centrifuged to get the cell pellet. Sphere cells were pelleted in the
827 sphere medium and then washed with PBS. Cell pellets were lysed in 9M urea lysis buffer by
828 sonication. The lysates were centrifuged at 12,000 g for 15 min, and the cleared supernatant was
829 collected. The protein concentration of the lysates was estimated using the BCA method, and 3 mg

830 protein from both monolayer and sphere cultures was pooled. Proteins were reduced using 5mM
831 dithiothreitol at 56°C for 45 min. Proteins were further alkylated using iodoacetamide at a final
832 concentration of 10mM and incubated the lysate at room temperature in the dark for 30 min.
833 Lysates were diluted to obtain a final urea concentration of <2 M using HEPES buffer. Sequencing
834 grade trypsin was added to achieve an enzyme to substrate ratio of 1:20 (w/w). Trypsin digestion
835 was carried out overnight at 37°C. The peptide digest was acidified using trifluoroacetic acid
836 (TFA) at a final concentration of 1%. The acidified peptide digest was centrifuged at 4,500 g for
837 15 min, and the supernatant was desalted using a C18 Sep-Pak cartridge. The desalted peptide
838 digest was frozen and lyophilized for 48 hrs. The lyophilized peptides were reconstituted in 7mM
839 Triethylammonium bicarbonate buffer (pH 9). Peptides were fractionated into 12 fractions using
840 basic reverse phase chromatography. The samples were dried at 4°C and reconstituted in 100 µl of
841 5% 2, 5-dihydroxybenzoic acid (DHB). TiO_2 beads (GL Sciences, Inc., Japan Catalogue # 5020-
842 75010) were washed in 5% DHB solution for 15 min. For each fraction, 2 µl of beads was added
843 to achieve the TiO_2: peptide ratio of 1:1 and incubated on a rotator for 15 min at room temperature.
844 The vials were centrifuged at 1,500 g for 1 min, and the supernatant with unbound peptides was
845 discarded. The beads were reconstituted in 5% DHB solution and loaded on to C8 Stage Tip. The
846 beads were washed twice with 100 µl of 80% acetonitrile with 1% TFA. The phosphopeptides
847 were eluted from TiO_2 beads using 30 µl of 2% NH_4OH solution, pH 10.5 (prepared by dissolving
848 20 µl of NH_4OH in 1 ml of 40% ACN) into collection tubes containing 20 µl of 0.1% TFA. Then,
849 the phosphopeptides were analyzed using hybrid LTQ–OrbitrapVelos ETD.

850 ## LC-MS/MS analysis

851 Samples were analyzed on a hybrid LTQ–Orbitrap Velos (Thermo Scientific, Bremen,
852 Germany) mass spectrometer equipped with a nanoelectrospray ion source interfaced with an Easy
853 nano-LC (Thermo Scientific, Bremen, Germany) for sample delivery. The samples were loaded on
854 to a 2 cm trap column (75 µm ID; Magic C 18 AQ, 5µm, 100 Å, Michrom Bioresources Inc.) using
855 1% formic acid with a flow rate of 3 µl/min and further resolved on a 15 cm analytical column (75
856 µm ID; Magic C 18 AQ, 3µm, 100 Å, Michrom Bioresources Inc., USA) using a 100-minute
857 gradient from 5% to 30% acetonitrile in 0.1% formic acid with a flow rate of 350 nl/min before
858 introducing into the mass spectrometer. The spray voltage was set to 2.2 kV while the capillary
859 temperature was set to 250°C. The MS instrument was operated in data-dependent acquisition
860 mode. A survey scan from m/z 350–1,700 was acquired in the Orbitrap with resolution 60,000 with
861 a maximum AGC target value of 1,000,000 ions. The fifteen most intense peptide ions with charge
862 states ≥2 were sequentially isolated to a target value of 50,000 ions and fragmented in the higher-
863 energy collisional dissociation (HCD) cell using 39% normalized collision energy. The maximum
864 ion injection times for MS and MS/MS were set to 100 ms and 200 ms, respectively. Fragment ion
865 spectra were detected in the Orbitrap mass analyzer with a resolution of 7,500. For all
866 measurements with the Orbitrap detector, a lock-mass ion from ambient air (m/z 445.120025) was
867 used for internal calibration.

868 ## Data analysis

869 The mass spectrometry-derived data were searched against the Human RefSeq database
870 (Version 52) using SEQUEST and Mascot search algorithms through Proteome Discoverer
871 software (Version 1.4.1.14) (Thermo Scientific, Bremen, Germany). The protease was specified as

872 trypsin and a maximum of 1 missed cleavage was allowed. Carbamidomethylation of cysteine was
873 set as a fixed modification while oxidation of methionine, phosphorylation at serine, threonine,
874 and tyrosine, and SILAC-labelling ($^{13}C_6$) at lysine and arginine were set as variable modifications.
875 MS and MS/MS mass tolerances were set to 10 ppm and 0.05 Da, respectively. Peptide
876 identification was based on a 1% false discovery rate calculated using target-decoy database
877 searches. The SILAC ratio for each peptide-spectrum match (PSM) was calculated by the
878 quantitation node and the peptides with ratios greater than two-fold were considered as
879 differentially regulated and were considered for further bioinformatics analysis.

880 Bioinformatic analysis

881 The phosphoproteins identified with <0.5 fold and >2 fold were considered as regulated
882 molecules. The two biological replicates were analyzed separately for pathway enrichment using
883 Genespring Version B13.0. A single Experiment Analysis with 700 source pathways identified the
884 regulated pathways and the molecules regulated in each pathway. All the pathways with $p<0.05$
885 were considered as significantly regulated. A Venn diagram of the significantly regulated pathways
886 from the biological replicates identified consistently regulated pathways. The list of regulated
887 molecules in each pathway was used to study the overlap of pathways.

888 Western blotting

889 Cell lysate was prepared using lysis buffer (0.15 M Sodium chloride, 0.025M Tris, 0.001
890 M EDTA, 0.5% (v/v) NP40, 0.5% (v/v) Triton X 100, 5% glycerol (v/v), 1× protease inhibitor, pH
891 7.4). The tumor lysate was prepared using RIPA buffer (150mM NaCl, 1% (v/v) NP40, 0.5% (v/v)
892 Sodium deoxycholate, 1% (v/v) SDS, 50mM Sodium orthovanadate, 10mM Sodium Fluoride).
893 The proteins were resolved using SDS-PAGE, followed by the wet-transfer of proteins to a

894 nitrocellulose membrane. After a 10 minutes wash with TBST (500 mM Tris, 1.5M NaCl, 0.15%
895 (v/v) Tween 20), the membrane was blocked using 3% BSA or 10% milk for 1 hour. Then, the
896 membrane was incubated with the primary antibody overnight at 4 ºC. The next day, the membrane
897 was washed thrice with TBST to remove unbound primary antibody and incubated in secondary
898 antibody for 1 hour at room temperature. After three times washing with TBST, the membrane was
899 developed using ECL reagent (Bio-Rad Laboratories, Hercules, California, USA).

900 Immunofluorescence (IF)/Immunohistochemistry (IHC)

901 Oral cancer cells were grown as monolayer or spheres for 3 days on confocal dishes. Then,
902 the cells were washed with PBS and fixed using 4% paraformaldehyde (PFA) for 10 minutes. The
903 cells were permeabilized and blocked with 2% fetal bovine serum (FBS) in PBS for surface
904 proteins or with 2% FBS in PBST, which contained 0.3% (v/v) Triton X-100 for intra-cellular
905 molecules for 0.5-1 hour. After removing blocking, cells were incubated with the primary antibody
906 overnight 4 ºC. The next day, cells were washed and incubated with the secondary antibody for 1
907 hour. Then, nuclei were stained using DAPI and washed with PBS to remove excess antibody and
908 DAPI. Further, cells were mounted with ProLong™ Gold Antifade Mountant (ThermoFisher
909 Scientific, Waltham, Massachusetts, USA) and imaged with a confocal microscope, Olympus
910 FV3000 or Nikon A1R LSCM.

911 Oral cancer patient samples were collected and fixed with 4% PFA for 1 day, followed by
912 storage in 30% sucrose solution. Then, 5µm sections were taken using the LeicaCM1850UV
913 Cryostat. The antigen unmasking was done using 0.01M Citrate buffer, pH 6.0. The IHC staining
914 protocol was similar to IF that used for cultured cells.

915 ## Fluorescence Activated Cell Sorting (FACS)

916 Cells were trypsinized and resuspended the pellet in DMEM with 10% FBS. Then, the cells
917 were kept inside a CO2 incubator for 1 hour for re-expression, when analyzed for membrane
918 markers. Then, cells were pelleted and fixed with 4% PFA for 10 minutes. After PBS wash, cells
919 were incubated with Alexa fluor-488 tagged primary antibodies for 1 hour at room temperature.
920 Then, after PBS wash, re-suspended the pellet in PBS, filtered with a cell strainer, and used for
921 FACS analysis using FACS AriaIII.

922 Oral cancer cells stably expressing ALDH1A1-DsRed2 were used for analyzing CSCs, as
923 reported before (32, 33). Briefly, the stable cells were selected using G418 selection. The 2-4% of
924 CSC reporting cells were sorted out, and the enriched population was maintained in DMEM
925 containing 20ng/ml G418. Oral cancer cells stably expressing ALDH1A1 DsRed2 (reporter cell
926 lines) with or without EPHA2/ Ephrin-B1 knock-down were trypsinized and re-suspended the
927 pellet in PBS, filtered with a cell strainer, and analyzed in FACS AriaIII.

928 ## Co-Immunoprecipitation (Co-IP) experiments

929 For Co-IP, we conjugated protein A/G bead (ThermoFisher Scientific, Waltham,
930 Massachusetts, USA) with the specific antibody or IgG antibodies for 5 hours. We prepared cell
931 lysate using lysis buffer (0.15 M Sodium chloride, 0.025M Tris, 0.001 M EDTA, 0.5% (v/v) NP40,
932 0.5% (v/v) Triton X 100, 5% glycerol (v/v), 1X protease inhibitor, pH 7.4). Cell lysate was
933 quantified using DC protein assay (Bio-Rad Laboratories, Hercules, California, USA) and 1 mg
934 precleared cell lysate was added to bead-antibody conjugate or bead-IgG conjugate and incubated
935 overnight at 4 ºC. The next day, the protein-antibody complex was eluted using 5X loading dye
936 for western blotting experiments or eluted after overnight incubation with IP elution buffer (0.15M

937 Sodium chloride, 0.2M Tris, 0.002 M EDTA, 1% (v/v) Triton X 100, 0.01% (v/v) SDS, 1X protease
938 inhibitor, pH 8.0) for *in vitro* kinase assay.

939 ShRNA lentiviral particles and infection

940 The lentiviral particles for Scrambled (shRNA Control), EPHA2, or Ephrin-B1 shRNA
941 were purchased from Santa Cruz Biotechnology, Inc., Dallas, Texas. These lentiviral particles
942 contain a mixture of three target-specific constructs that encode 19-25 nucleotides (plus hairpin)
943 shRNA designed to knock down the expression of that specific gene. One day before infection,
944 cells were seeded in a 24-well plate. On the day of infection, fresh medium containing 20ug/ml
945 sequabrene was added to cells. Then, 6-10×10^4 *ifu/ml* of viral shRNA particles were directly added
946 to that medium. This infection procedure was repeated the next day as well. Then, the LV-shRNA-
947 infected cells were selected using puromycin antibiotic (200 ng/ml).

948 FRET facilitated photoswitching

949 PSmOrange-C1 and mT-Sapphire-C1 plasmids were used as pairs for FRET facilitated
950 photoswitching. Then, PSmOrange-C1-EPHA2 or mT-Sapphire-C1-Ephrin-B1 were cloned by
951 amplifying *EPHA2* from pCLXSN-EPHA2 Flag plasmid or *EFNB1* from FUW-ubiquitin-Ephrin-
952 B1-SV40-RFP (biR) plasmid using PrimeSTAR® Max Premix (2X) DNA polymerase mix (Takara
953 Bio Inc., Kusatsu, Shiga, Japan), respectively, using primers with restriction digestion sites, SalI
954 and SmaI. Primers for *EPHA2* were F: 5'-GCATCCCGGGTTAGTCGTCATCCTTG-3', R: 5'-
955 ATATGTCGACTACCTCGAGATGGAGC-3'. Primers for *EFNB1* were F: 5'
956 ACATGTCGACCAGGATCTCCACATGGC-3', R: 5'- ACATCCCGGGCGCGATATCTCAAAC-
957 3'. Then, the backbone and the PCR products were cut and eluted from the gel using the Gel and
958 PCR clean up kit (Macherey-Nagel, Düren, Germany). Further, they were used for ligation reaction

959 using T4 DNA Ligase (ThermoFisher Scientific, Waltham, Massachusetts, USA) for overnight at
960 4 ºC. Then, the ligated product was transformed into DH5α *E. coli* cells. Then, positive clones
961 were confirmed using restriction digestion and sequencing. Further, HSC-4 cells were transiently
962 transfected with PSmOrange C1-EPHA2 and mT-Sapphire C1-Ephrin-B1 plasmids using
963 Lipofectamine-3000 (ThermoFisher Scientific, Waltham, Massachusetts, USA). Then, these cells
964 were grown in sphere condition for 3 days. Then, we imaged FRET facilitated photoswitching in
965 live cells where we performed a sequential acquisition, as Ex. 639 nm/ Em. 650/25 nm, Ex. 560
966 nm/ Em. 575/30 nm, Ex. 405 nm/ Em. 488/40 nm. Further, a pulse of 30 iterations of excitation at
967 405 nm was given. Then, the next cycle was Ex. 639 nm/ Em. 650/25 nm, Ex. 560 nm/ Em. 575/30
968 nm.

969 Proximity Ligation Assay (PLA)

970 We used Oral cancer cells were grown as spheres for 3 days in confocal dishes. PLA was
971 performed using Duolink® In Situ Red Starter Kit Mouse/Rabbit (Sigma-Aldrich, St. Louis,
972 Missouri, USA). Briefly, the cells were washed with PBS and fixed using 4% paraformaldehyde
973 (PFA) for 10 minutes. Followed by fixation, the cell membrane was stained with wheat germ
974 agglutinin (WGA) Alexa fluor 488 (5µg/ml). Then, cells were permeabilized with 0.5% fetal
975 bovine serum (FBS) in PBST, which contained 0.3% (v/v) Triton X-100 for 30 minutes. Then,
976 cells were washed with PBS and the added the blocking solution. After removing blocking, cells
977 were incubated in primary antibodies (raised in mouse and rabbit, respectively) overnight at 4 ºC.
978 The next day, cells were washed and incubated with the PLA probes for 1 hour at 37 ºC. Then,
979 PLA probes were removed, and cells were washed with PBS. Subsequently, cells were incubated
980 with ligase for 30 minutes, followed by incubation with polymerase for 1 hour 40 minutes at 37

ºC. Further, cells were mounted with mounting medium containing DAPI and imaged with a confocal microscope, Olympus FV3000.

In vitro kinase assay

The Universal Kinase Activity Kit (R&D Systems, Minneapolis, Minnesota, USA) contains ATP, coupling phosphatase (CD39L2), ADP, and malachite green reagents. The assay was performed with mixing varying concentration of EPHA2 kinase obtained from eluate of the co-immunoprecipitation with either Anti-EPHA2, IgG or bead-only control and a small stretch of synthesized peptides with specific tyrosine residues (S BioChem, India) which acted as the acceptor (2mM), ATP (1mM) and CD39L2 (10 ng/µl) followed with 10 minutes' incubation at room temperature. Further, malachite green reagents were added, which form a green color upon kinase activity, which was read at 655 nm using an ELISA Plate Reader (Bio-Rad Laboratories, Hercules, California, USA). Negative control for the kinase assay lacked the kinase (IP eluate). Peptides used were YVDPHTYEDPNQ, which contains autophosphorylation residues (Y588 and Y594) of EPHA2, GDYGHPVYIVQEMPPQ, which contains Y324 and Y329 residues of Ephrin-B1, and NYCPHYEKVSG, which contains Y317 residue of Ephrin-B1.

Extreme Limiting Dilution Assay (ELDA)

For *in vitro* sphere formation assay, cells were trypsinized and the serial dilutions were prepared and seeded in non-adherent 96-well plate (coated with 1% Poly (2-hydroxyethyl methacrylate) or polyHEMA to deplete adherence of the plate) in sphere medium and maintained for 6 days, supplementing medium every other day. On the 6th day, counted the spheres in each well and data was used for Extreme limiting dilution assay (ELDA, (https://bioinf.wehi.edu.au/software/elda/). CSC frequency was calculated using ELDA analysis,

1003 which is a web-tool available online, and designed by the Bioinformatics Division, The Walter and
1004 Eliza Hall Institute of Medical Research in Australia. ELDA plotted a log-fraction plot, the slope
1005 of which gives CSC frequency.

1006 NOD.CB17-Prkdc^{scid}I12rg^{tm1Wjl}/SzJ (NSG) mice were used for generating tumors for *in vivo* serial
1007 dilution xenograft assay, following approved protocols from IAEC. Cells were serially diluted and
1008 mixed with Corning® Matrigel® Growth Factor Reduced (GFR) Basement Membrane Matrix and
1009 injected subcutaneously on the flanks of the mice. After palpable tumors were formed, the tumors
1010 were collected and representative images were taken. CSC frequency was calculated using ELDA.

1011 Site-directed mutagenesis

1012 Site-directed mutagenesis of tyrosine to phenylalanine in Ephrin-B1 RFP plasmid (Ephrin-
1013 B1 and RFP are activated under two different promoters, Ephrin-B1 under UBQ promoter and RFP
1014 under SV40 promoter respectively) was done using PfuUltra II Fusion HS DNA Polymerase
1015 (Agilent Technologies, Inc., Santa Clara, California, USA) with completely complimentary
1016 primers of length between 26-35 base pairs which occupies mutated base at the centre of the
1017 primers. Primers for Ephrin-B1 Y323F are F: 5'-GTGAGTGGGGAC TTCGGGCATCCTGTC-3',
1018 R: 5'- GACAGGATGCCCGAAGTCCCCACTCAC-3'. Primers for Ephrin-B1 Y316F are F: 5'-
1019 TACTGCCCCCACTTTGAGAAGGTGAGTG-3', R: 5'-
1020 CACTCACCTTCTCAAAGTGGGGGCAGTA-3'. After PCR amplification with the mutated
1021 primers, the PCR product was digested with the DpnI enzyme and performed transformation into
1022 DH5α E. Coli cells. Positive clones were confirmed with restriction digestion and sequencing
1023 reaction.

1024 Orthotopic models for oral carcinoma

1025 NOD.CB17-*Prkdc*^{scid}/J (SCID) or NOD.CB17-Prkdc^{scid}I12rg^{tm1Wjl}/SzJ (NSG) mice were
1026 used for generating tumors following approved protocols from IAEC. For the *in vivo* serial dilution
1027 xenograft assay, 1x10^{6} cells of oral cancer cells were mixed with Corning® Matrigel® Growth
1028 Factor Reduced (GFR) Basement Membrane Matrix and injected subcutaneously on the flanks of
1029 the mice. Tumors were collected after 2-3 weeks and photographed. For the orthotopic model,
1030 1x10^{6} cells of oral cancer cells were mixed with Corning® Matrigel® Growth Factor Reduced
1031 (GFR) Basement Membrane Matrix and injected into the floor of the mouth region superficial to
1032 the mylohyoid muscle. The animals were periodically monitored for overall survival analysis. The
1033 weight of the animals and tumor volume were measured periodically (using digital Vernier
1034 calipers) for 10 weeks. The death of the animal or ethical endpoint (visible signs of pain or distress,
1035 or if the weight loss was >25% of pre-injection) was considered as the survival time.

1036 *In-silico* analysis of oral cancer patient data

1037 To analyze the pattern of expression of EPHA2, Ephrin-B1, and EPHB2 mRNA in oral
1038 cancer specimens, data was downloaded from the Gene Expression Omnibus data portal
1039 (https://www.ncbi.nlm.nih.gov/geo/). The GEO accession numbers of the datasets are GSE13601,
1040 GSE65858. The platform used for expression profiling in all three datasets were microarray. In
1041 GSE65858, a total of 300 samples were considered for analysis and quality control procedures
1042 were applied to microarray probe-level intensity files. A total of 255 tumor arrays remained after
1043 removing low-quality arrays, duplicate arrays, and arrays from non-HNSCC samples. Expression
1044 values were log2-transformed and normalized using RSN. The relative normalized log-
1045 transformed microarray data was used for all the analysis. The TCGA data (N=515) was accessed

1046 from the TCGA Research Network: https://www.cancer.gov/tcga (accessed on 15 November
1047 2021).

1048 Descriptive statistics were used for all clinical variables. The difference in gene expression levels
1049 was evaluated by the Mann–Whitney U test/Kruskal–Wallis test. Correlations were evaluated by
1050 Pearson's rank test. Heatmap analysis was also performed to analyze the association of various
1051 genes, EPHA2, Ephrin-B1 and EPHB2. Kaplan-Meier analysis was used to examine the estimated
1052 differences in overall survival between the various groups. Log-rank test (Mantel-Cox) was used
1053 to compare the survival between groups. Survival analysis was performed by stratifying tumors
1054 based on the upper or third quartile expression of EPHA2 and Ephrin-B1 mRNA levels and
1055 grouped into tumors with high and low expression. For all tests, a p-value of <0.05 was considered
1056 to be statistically significant. All statistical analysis was carried out using the software XLSTAT -
1057 version 2022.2.1.

1058 Tissue microarray (TMA) and IHC analysis

1059 Archival samples were collected from Cochin Cancer Research Centre (CCRC). Patients
1060 were categorized as recurrent and disease-free groups where patients with disease-free survival of
1061 less than 15 months were considered as recurrent (25 samples) while patients with disease-free
1062 survival for more than 15 months were considered as disease-free group (27 samples).

1063 Immunohistochemistry for the antibodies was done on each of the TMA sections as per
1064 standard protocol using the Ventana Benchmark^{XT} staining system (Ventana Medical Systems,
1065 Tucson, AZ, USA). Briefly, 5 µm thick sections were fixed in a hot air oven at 60°C for 60 min
1066 and loaded onto the IHC staining machine. De-paraffinization was performed using EZ Prep
1067 solution (Proprietary-Ventana reagent), and antigen retrieval was done using Cell Conditioning

solution 1 (CC1) for 60 min. The primary antibody was added manually and incubated for 32 min at room temperature. Optiview DAB Detection Kit (Ventana Medical Systems) was used to visualize the signal, using DAB (3–3′diaminobenzidine) as the chromogen. Further, the sections were automatically counterstained with hematoxylin II (Ventana Medical Systems) for 12 min. The slides were removed from the autostainer, washed in de-ionized water, dehydrated in graded ethanol, cleared in xylene, and examined by microscopy. Appropriate positive and negative controls were run for each batch. Two pathologists scored the staining independently. Nuclear/cytoplasmic staining in more >1% of tumor cells was considered positive. Data from 24 recurrent and 26 disease-free samples were used for the statistical analysis.

Acknowledgements

We acknowledge Akhilesh Pandey and the Proteomic facility of Institute of Bioinformatics, Bangalore, for the proteomic analyses. The contribution of Annie Agnes Suganya S for Fig 1C is acknowledged. We thank the contributions of the Animal Research Facility, the Confocal Facility and FACS Facility of RGCB. Reshma Raj R received funding from Council of Scientific & Industrial Research, India (09/716(0188)/2019-EMR-I). The work was financially supported by the funding from DST-SERB (SR/S0/HS/0133/2010), DBT (BT/PR14379/Med/30/536/2010), and RGCB LRF.

References

1. Pasquale EB. Eph receptors and ephrins in cancer progression. Nat Rev Cancer. 2024;24(1):5-27.

1090 2. Mann F, Harris WA, Holt CE. New views on retinal axon development: a navigation guide.
1091 Int J Dev Biol. 2004;48(8-9):957-64.
1092 3. Medori M, Spelzini G, Scicolone G. Molecular complexity of visual mapping: a challenge
1093 for regenerating therapy. Neural Regen Res. 2020;15(3):382-9.
1094 4. Mellitzer G, Xu Q, Wilkinson DG. Eph receptors and ephrins restrict cell intermingling
1095 and communication. Nature. 1999;400(6739):77-81.
1096 5. Arthur A, Koblar S, Shi S, Gronthos S. Eph/ephrinB mediate dental pulp stem cell
1097 mobilization and function. J Dent Res. 2009;88(9):829-34.
1098 6. Goichberg P, Bai Y, D'Amario D, Ferreira-Martins J, Fiorini C, Zheng H, et al. The ephrin
1099 A1-EphA2 system promotes cardiac stem cell migration after infarction. Circ Res.
1100 2011;108(9):1071-83.
1101 7. Batlle E, Henderson JT, Beghtel H, van den Born MM, Sancho E, Huls G, et al. Beta-
1102 catenin and TCF mediate cell positioning in the intestinal epithelium by controlling the expression
1103 of EphB/ephrinB. Cell. 2002;111(2):251-63.
1104 8. Ottone C, Krusche B, Whitby A, Clements M, Quadrato G, Pitulescu ME, et al. Direct cell-
1105 cell contact with the vascular niche maintains quiescent neural stem cells. Nat Cell Biol.
1106 2014;16(11):1045-56.
1107 9. Chen K, Bai H, Liu Y, Hoyle DL, Shen WF, Wu LQ, et al. EphB4 forward-signaling
1108 regulates cardiac progenitor development in mouse ES cells. J Cell Biochem. 2015;116(3):467-75.
1109 10. Arthur A, Nguyen TM, Paton S, Zannettino ACW, Gronthos S. Loss of EfnB1 in the
1110 osteogenic lineage compromises their capacity to support hematopoietic stem/progenitor cell
1111 maintenance. Exp Hematol. 2019;69:43-53.
1112 11. Yi K, Chen W, Zhou X, Xie C, Zhong C, Zhu J. Bisphenol S exposure promoted stemness
1113 of triple-negative breast cancer cells via regulating Gli1-mediated Sonic hedgehog pathway.
1114 Environ Res. 2024:120293.
1115 12. Marquardt T, Shirasaki R, Ghosh S, Andrews SE, Carter N, Hunter T, et al. Coexpressed
1116 EphA receptors and ephrin-A ligands mediate opposing actions on growth cone navigation from
1117 distinct membrane domains. Cell. 2005;121(1):127-39.
1118 13. Kao TJ, Kania A. Ephrin-mediated cis-attenuation of Eph receptor signaling is essential for
1119 spinal motor axon guidance. Neuron. 2011;71(1):76-91.
1120 14. Falivelli G, Lisabeth EM, Rubio de la Torre E, Perez-Tenorio G, Tosato G, Salvucci O, et
1121 al. Attenuation of eph receptor kinase activation in cancer cells by coexpressed ephrin ligands.
1122 PLoS One. 2013;8(11):e81445.
1123 15. Cecchini A, Cornelison DDW. Eph/Ephrin-Based Protein Complexes: The Importance of
1124 cis Interactions in Guiding Cellular Processes. Front Mol Biosci. 2021;8:809364.
1125 16. Guo X, Yang Y, Tang J, Xiang J. Ephs in cancer progression: complexity and context-
1126 dependent nature in signaling, angiogenesis and immunity. Cell Commun Signal. 2024;22(1):299.
1127 17. Biao-xue R, Xi-guang C, Shuan-ying Y, Wei L, Zong-juan M. EphA2-dependent molecular
1128 targeting therapy for malignant tumors. Curr Cancer Drug Targets. 2011;11(9):1082-97.
1129 18. Liu W, Yu C, Li J, Fang J. The Roles of EphB2 in Cancer. Front Cell Dev Biol.
1130 2022;10:788587.
1131 19. Pergaris A, Danas E, Goutas D, Sykaras AG, Soranidis A, Theocharis S. The Clinical
1132 Impact of the EPH/Ephrin System in Cancer: Unwinding the Thread. Int J Mol Sci. 2021;22(16).
1133 20. Qiu C, Sun N, Zeng S, Chen L, Gong F, Tian J, et al. Unveiling the therapeutic promise of
1134 EphA2 in glioblastoma: a comprehensive review. Discov Oncol. 2024;15(1):501.

1135 21. Veiga RN, de Azevedo ALK, de Oliveira JC, Gradia DF. Targeting EphA2: a promising
1136 strategy to overcome chemoresistance and drug resistance in cancer. J Mol Med (Berl).
1137 2024;102(4):479-93.
1138 22. Binda E, Visioli A, Giani F, Lamorte G, Copetti M, Pitter KL, et al. The EphA2 receptor
1139 drives self-renewal and tumorigenicity in stem-like tumor-propagating cells from human
1140 glioblastomas. Cancer Cell. 2012;22(6):765-80.
1141 23. Song W, Ma Y, Wang J, Brantley-Sieders D, Chen J. JNK signaling mediates EPHA2-
1142 dependent tumor cell proliferation, motility, and cancer stem cell-like properties in non-small cell
1143 lung cancer. Cancer Res. 2014;74(9):2444-54.
1144 24. Li JY, Xiao T, Yi HM, Yi H, Feng J, Zhu JF, et al. S897 phosphorylation of EphA2 is
1145 indispensable for EphA2-dependent nasopharyngeal carcinoma cell invasion, metastasis and stem
1146 properties. Cancer Lett. 2019;444:162-74.
1147 25. Bai J, Chen Y, Sun Y, Wang X, Wang Y, Guo S, et al. EphA2 promotes the transcription of
1148 KLF4 to facilitate stemness in oral squamous cell carcinoma. Cell Mol Life Sci. 2024;81(1):278.
1149 26. Zhao P, Sun J, Huang X, Zhang X, Liu X, Liu R, et al. Targeting the KLF5-EphA2 axis can
1150 restrain cancer stemness and overcome chemoresistance in basal-like breast cancer. Int J Biol Sci.
1151 2023;19(6):1861-74.
1152 27. Hamaoka Y, Negishi M, Katoh H. Tyrosine kinase activity of EphA2 promotes its S897
1153 phosphorylation and glioblastoma cell proliferation. Biochem Biophys Res Commun.
1154 2018;499(4):920-6.
1155 28. Stokowski A, Shi S, Sun T, Bartold PM, Koblar SA, Gronthos S. EphB/ephrin-B interaction
1156 mediates adult stem cell attachment, spreading, and migration: implications for dental tissue repair.
1157 Stem Cells. 2007;25(1):156-64.
1158 29. Zhu L, Dissanayaka WL, Green DW, Zhang C. Stimulation of EphB2/ephrin-B1 signalling
1159 by tumour necrosis factor alpha in human dental pulp stem cells. Cell Prolif. 2015;48(2):231-8.
1160 30. Catchpole T, Henkemeyer M. EphB2 tyrosine kinase-dependent forward signaling in
1161 migration of neuronal progenitors that populate and form a distinct region of the dentate niche. J
1162 Neurosci. 2011;31(32):11472-83.
1163 31. Mencucci MV, Lapyckyj L, Rosso M, Besso MJ, Belgorosky D, Isola M, et al. Ephrin-B1
1164 Is a Novel Biomarker of Bladder Cancer Aggressiveness. Studies in Murine Models and in Human
1165 Samples. Front Oncol. 2020;10:283.
1166 32. Dharmapal D, Jyothy A, Mohan A, Balagopal PG, George NA, Sebastian P, et al. beta-
1167 Tubulin Isotype, TUBB4B, Regulates The Maintenance of Cancer Stem Cells. Front Oncol.
1168 2021;11:788024.
1169 33. Shanmugam G, Mohan A, Kumari K, Louis JM, Soumya Krishnan U, Balagopal PG, et al.
1170 A novel reporter construct for screening small molecule inhibitors that specifically target self-
1171 renewing cancer cells. Exp Cell Res. 2019;383(2):111551.
1172 34. Hu Y, Smyth GK. ELDA: extreme limiting dilution analysis for comparing depleted and
1173 enriched populations in stem cell and other assays. J Immunol Methods. 2009;347(1-2):70-8.
1174 35. Ai HW, Hazelwood KL, Davidson MW, Campbell RE. Fluorescent protein FRET pairs for
1175 ratiometric imaging of dual biosensors. Nat Methods. 2008;5(5):401-3.
1176 36. Sarkar M, Raj RR, Maliekal TT. Finding the partner: FRET and beyond. Exp Cell Res.
1177 2024;441(2):114166.

1178 37. Subach OM, Cranfill PJ, Davidson MW, Verkhusha VV. An enhanced monomeric blue
1179 fluorescent protein with the high chemical stability of the chromophore. PLoS One.
1180 2011;6(12):e28674.
1181 38. Jain S, Dhall K, Brar GS, Gupta S, Jain K, Garg N, et al. Outcome of Upfront Surgically
1182 Resected Patients of Oral Tongue Squamous Cell Carcinoma and Factors Affecting it: Experience
1183 from Tertiary Care Facility in North India. Indian J Otolaryngol Head Neck Surg.
1184 2024;76(5):4479-86.
1185 39. Lee YJ, Jung SP, Bae JW, Yang SM, You JY, Bae SY. Prognosis according to the timing of
1186 recurrence in breast cancer. Ann Surg Treat Res. 2023;104(1):1-9.
1187 40. Zhao H, Chen Z, Fang Y, Su M, Xu Y, Wang Z, et al. Prediction of Prognosis and
1188 Recurrence of Bladder Cancer by ECM-Related Genes. J Immunol Res. 2022;2022:1793005.
1189 41. Jeong WG, Choi H, Chae KJ, Kim J. Prognosis and recurrence patterns in patients with
1190 early stage lung cancer: a multi-state model approach. Transl Lung Cancer Res. 2022;11(7):1279-
1191 91.
1192 42. Wang B, Zhang S, Yue K, Wang XD. The recurrence and survival of oral squamous cell
1193 carcinoma: a report of 275 cases. Chin J Cancer. 2013;32(11):614-8.
1194 43. Davaatsend O, Altannamar M, Ganbat M, Jagdagsuren U. Factors associated with
1195 recurrence in patients with oral cancer in Mongolia. BMC Cancer. 2024;24(1):356.
1196 44. Mirshahidi S, Yuan IJ, Chen Z, Simental A, Lee SC, Andrade Filho PA, et al. Tumor Cell
1197 Stemness and Stromal Cell Features Contribute to Oral Cancer Outcome Disparity in Black
1198 Americans. Cancers (Basel). 2024;16(15).
1199 45. Banki M, Moosavi MS. Umbrella Review on Cancer Stem Cell in Oral and Head and Neck
1200 Squamous Cell Carcinoma. J Stem Cells Regen Med. 2023;19(2):29-33.
1201 46. Castellvi J, Garcia A, de la Torre J, Hernandez J, Gil A, Xercavins J, et al. Ephrin B
1202 expression in epithelial ovarian neoplasms correlates with tumor differentiation and angiogenesis.
1203 Hum Pathol. 2006;37(7):883-9.
1204 47. Sawai Y, Tamura S, Fukui K, Ito N, Imanaka K, Saeki A, et al. Expression of ephrin-B1 in
1205 hepatocellular carcinoma: possible involvement in neovascularization. J Hepatol. 2003;39(6):991-
1206 6.
1207 48. Hu Y, Xie Q, Zhao J, Yang R, Qin J, Li H, et al. Interaction between the EPHB2 receptor
1208 and EFNB1 ligand drives gastric cancer invasion and metastasis via the Wnt/beta-catenin/FAK
1209 pathway. Int J Biol Macromol. 2024;258(Pt 1):128848.
1210 49. Phan NN, Liu S, Wang CY, Hsu HP, Lai MD, Li CY, et al. Overexpressed gene signature
1211 of EPH receptor A/B family in cancer patients-comprehensive analyses from the public high-
1212 throughput database. Int J Clin Exp Pathol. 2020;13(5):1220-42.
1213 50. Zhao C, Wang A, Lu F, Chen H, Fu P, Zhao X, et al. Overexpression of junctional adhesion
1214 molecule-A and EphB2 predicts poor survival in lung adenocarcinoma patients. Tumour Biol.
1215 2017;39(2):1010428317691000.
1216 51. Leung HW, Leung CON, Lau EY, Chung KPS, Mok EH, Lei MML, et al. EPHB2 Activates
1217 beta-Catenin to Enhance Cancer Stem Cell Properties and Drive Sorafenib Resistance in
1218 Hepatocellular Carcinoma. Cancer Res. 2021;81(12):3229-40.
1219 52. Kim H, Myung JK, Paik SS, Kim H, Park H, Kim YJ, et al. EPHB2 expression is associated
1220 with intestinal phenotype of gastric cancer and indicates better prognosis by suppressing gastric
1221 cancer migration. Am J Cancer Res. 2022;12(3):1295-308.

1222 53. Ebrahim AS, Hailat Z, Bandyopadhyay S, Neill D, Kandouz M. The Value of EphB2
1223 Receptor and Cognate Ephrin Ligands in Prognostic and Predictive Assessments of Human Breast
1224 Cancer. Int J Mol Sci. 2021;22(15).
1225 54. Jang BG, Kim HS, Chang WY, Bae JM, Kang GH. Prognostic Significance of EPHB2
1226 Expression in Colorectal Cancer Progression. J Pathol Transl Med. 2018;52(5):298-306.
1227 55. Kakarla M, ChallaSivaKanaka S, Dufficy MF, Gil V, Filipovich Y, Vickman R, et al. Ephrin
1228 B Activate Src Family Kinases in Fibroblasts Inducing Stromal Remodeling in Prostate Cancer.
1229 Cancers (Basel). 2022;14(9).
1230 56. Gehring MP, Pasquale EB. Protein kinase C phosphorylates the EphA2 receptor on serine
1231 892 in the regulatory linker connecting the kinase and SAM domains. Cell Signal.
1232 2020;73:109668.
1233 57. Miao H, Li DQ, Mukherjee A, Guo H, Petty A, Cutter J, et al. EphA2 mediates ligand-
1234 dependent inhibition and ligand-independent promotion of cell migration and invasion via a
1235 reciprocal regulatory loop with Akt. Cancer Cell. 2009;16(1):9-20.
1236 58. Zhou Y, Yamada N, Tanaka T, Hori T, Yokoyama S, Hayakawa Y, et al. Crucial roles of
1237 RSK in cell motility by catalysing serine phosphorylation of EphA2. Nat Commun. 2015;6:7679.
1238 59. Finney AC, Scott ML, Reeves KA, Wang D, Alfaidi M, Schwartz JC, et al. EphA2 signaling
1239 within integrin adhesions regulates fibrillar adhesion elongation and fibronectin deposition. Matrix
1240 Biol. 2021;103-104:1-21.
1241 60. Xiang YP, Xiao T, Li QG, Lu SS, Zhu W, Liu YY, et al. Y772 phosphorylation of EphA2
1242 is responsible for EphA2-dependent NPC nasopharyngeal carcinoma growth by Shp2/Erk-1/2
1243 signaling pathway. Cell Death Dis. 2020;11(8):709.
1244 61. Lechtenberg BC, Gehring MP, Light TP, Horne CR, Matsumoto MW, Hristova K, et al.
1245 Regulation of the EphA2 receptor intracellular region by phosphomimetic negative charges in the
1246 kinase-SAM linker. Nat Commun. 2021;12(1):7047.
1247 62. Fang WB, Brantley-Sieders DM, Hwang Y, Ham AJ, Chen J. Identification and functional
1248 analysis of phosphorylated tyrosine residues within EphA2 receptor tyrosine kinase. J Biol Chem.
1249 2008;283(23):16017-26.
1250 63. Fujikawa K, Inoue Y, Sakai M, Koyama Y, Nishi S, Funada R, et al. Vav3 is regulated
1251 during the cell cycle and effects cell division. Proc Natl Acad Sci U S A. 2002;99(7):4313-8.
1252 64. Kalo MS, Yu HH, Pasquale EB. In vivo tyrosine phosphorylation sites of activated ephrin-
1253 B1 and ephB2 from neural tissue. J Biol Chem. 2001;276(42):38940-8.
1254 65. Yin Y, Yamashita Y, Noda H, Okafuji T, Go MJ, Tanaka H. EphA receptor tyrosine kinases
1255 interact with co-expressed ephrin-A ligands in cis. Neurosci Res. 2004;48(3):285-96.
1256 66. Liu SQ, Cheng XX, He S, Xia T, Li YQ, Peng W, et al. Super-enhancer-driven EFNA1
1257 fuels tumor progression in cervical cancer via the FOSL2-Src/AKT/STAT3 axis. J Clin Invest.
1258 2025;135(8).
1259 67. Cortina C, Palomo-Ponce S, Iglesias M, Fernandez-Masip JL, Vivancos A, Whissell G, et
1260 al. EphB-ephrin-B interactions suppress colorectal cancer progression by compartmentalizing
1261 tumor cells. Nat Genet. 2007;39(11):1376-83.
1262 68. Kristiansen TZ, Harsha HC, Gronborg M, Maitra A, Pandey A. Differential membrane
1263 proteomics using 18O-labeling to identify biomarkers for cholangiocarcinoma. J Proteome Res.
1264 2008;7(11):4670-7.
1265 69. Harsha HC, Pinto SM, Pandey A. Proteomic strategies to characterize signaling pathways.
1266 Methods Mol Biol. 2013;1007:359-77.

1267 # Supporting information

1268 **S1 Fig. Sphere culture enriches self-renewing population.**

1269 (A) Serial passaging sphere formation assay with three oral cancer cells as indicated. 3D Spheres
1270 were formed up to three passages. The image indicates primary and tertiary spheres formed in the
1271 three oral cancer cells. (B) We performed a soft agar colony formation assay with three oral cancer
1272 cells grown as monolayer (ML) or 3D sphere (Sph). After 21 days, the colonies were counted at
1273 10X magnification, and the number of colonies/10 fields in monolayer and sphere from 3
1274 independent experiments were plotted as mean ± SD. (C) HSC-4 cells were grown as ML or Sph
1275 for 3 days. Then, we stained the cells with ALDH1A1 and Hoechst. (D) HSC-4 cells grown as
1276 monolayer or 3D spheres for 3 days were used for RNA isolation followed with RT-PCR (E) 3-
1277 Day-old HSC-4 ML or 3D Sph were used for cell lysis preparation followed by western blotting
1278 to check expression of OCT4A. Statistical analysis was done by an unpaired-two-tailed students
1279 t-test. ***, **** represents $p<0.001$ and $p<0.0001$ respectively.

1280 **S2 Fig. Diagrammatic representation of proteomic analyses.**

1281 (A) HSC-4 cells were grown as monolayer in SILAC medium containing heavy arginine and
1282 lysine, while HSC-4 3D sphere cells were maintained in sphere medium with normal amino acids
1283 for 6 days. The membrane prep was used for LC-MS/MS analysis, as shown in the diagram. (B)
1284 The cells were grown as described, and the lysates were used for phosphoproteomic analysis

1285 **S3 Fig. Validation of proteomic data.**

1286 (A) HSC-4 cells were grown in sphere conditions for 3 days, fixed, and stained for the indicated
1287 molecules. The scale bar represents 10µm. (B) Some of the molecules obtained from

1288 phosphoproteomic analysis were confirmed using western blotting using 6-Day-old monolayer
1289 (ML) or 3D Sphere (Sph). (C) The differentially expressed phospho enriched peptides obtained
1290 from the phosphoproteomic analysis were analyzed for pathway enrichment. The bar plot
1291 represents differential phosphorylation of the molecules in the Eph/Ephrin signaling pathway. (D)
1292 HSC-4 Cells were grown as monolayer or sphere for 3 days, and were used for FACS analysis to
1293 check surface expression of EPHA2, Ephrin-B1, and EPHB2 under non-permeabilizing condition.
1294 FITC-A represents the positivity of the indicated molecules.

1295 **S4 Fig. Western blots of EPHA2 and Ephrin-B1.**

1296 (A) Western blot experiment to show bands of EPHA2 (full blot) of HSC-4 oral cancer cells with
1297 knock-down of EPHA2. β-Actin was used as the loading control. (B) Bar plot represents fold
1298 change of knock-down over control in western blot experiment. (C) Bar plot represents fold change
1299 of knock-down over control in qRT-PCR experiment. (D) Western blot experiment to show bands
1300 of Ephrin-B1 in a full blot of HSC-4 oral cancer cells with knock-down of Ephrin-B1. (E) The Bar
1301 plot represents the fold change of knock-down over control in the western blot experiment. (F)
1302 The Bar plot represents the fold change of knock-down in the qRT-PCR experiment. Statistical
1303 analysis of 3 independent experiments was done by a paired-two-tailed students t-test. **, ***,
1304 **** represents $p<0.01$, $p<0.001$ and $p<0.0001$ respectively.

1305 **S5 Fig. Western blot of pEphrin-B1.**

1306 (A-B) Western blot experiment to show bands of pEphrin-B (Y324/329) and pEphrin-B1 Y317
1307 (full blot) of 3-Day-old HSC-4 3D spheres with knock-down of EPHA2. β-Actin was used as the
1308 loading control.

1309 **S6 Fig. Cloning of Ephrin-B1 Y324F or Ephrin-B1 Y317F.**

1310 (A-B) We performed site-directed mutagenesis of FUW-ubiquitin-Ephrin-B1-SV40-RFP plasmid.
1311 The Ephrin-B1 Y324F clone was confirmed by restriction digestion and sequencing, while the
1312 parent plasmid was used as the positive control.

1313 **S7 Fig. *In vitro* sphere formation assay (ELDA).**

1314 (A) Western blot confirmation of single knock-down of EPHA2 or Ephrin B1 and dual knock-
1315 down of both molecules. (B) We normalized the expression with β-Actin. Then the fold change
1316 was calculated by dividing relative expression in knock-down by control, and was plotted as mean
1317 ± SD values from 3 biological replicates. (C) The image shows the 6-Day spheres formed in the
1318 dilution of 3000 HSC-4 cells. The scale bar represented 100μm. The bar plot shows mean ± SD
1319 values of the total number of spheres formed per well for each dilution in single knock-down of
1320 EPHA2 in HSC-4 cells. The graph represents a log fraction plot obtained from ELDA analysis,
1321 and the slope of it represents cancer stem cell frequency. The table shows the data for ELDA
1322 analysis. (D) The bar plot shows mean ± SD values of the total number of spheres formed per well
1323 for each dilution in single knock-down and dual knock-down cells of RCB1015. (E) the table
1324 shows the data for the ELDA analysis of RCB1015. Statistical analysis other than ELDA was done
1325 by a paired-two-tailed students t-test. *, **, **** represents $p<0.05$, $p<0.01$ and $p<0.0001$
1326 respectively.

1327 **S8 Fig. ELDA for serial dilution xenograft and mutants.**

1328 (A-D) Table shows the data for ELDA analysis for the indicated combinations.

1329 **S9 Fig. Cloning of PSmOrange-C1 EPHA2 and mT-Sapphire-C1 Ephrin-B1.**

1330 (A) PSmOrange-C1-EPHA2 clone was confirmed using restriction digestion and sequencing.
1331 Restriction digestion was performed with enzymes SalI and SmaI. The expected band sizes were
1332 4697 for the backbone and 2972 for the insert. (B) mT-Sapphire-C1-Ephrin-B1 clone was
1333 confirmed using restriction digestion and sequencing. Restriction digestion was performed with
1334 enzymes SalI and SmaI. The expected band sizes were 4712 for the backbone and 1067 for the
1335 insert.

1336 **S10 Fig. FRET Facilitated photoswitching.**

1337 (A-C) HSC-4 cells were transiently transfected with empty vectors (PSmOrange-C1 and mT-
1338 Sapphire-C1) or with the PSmOrange C1-EPHA2 and mT-Sapphire-C1 Ephrin-B1. Then, these
1339 cells were grown as spheres for 3 days, followed by imaging for FRET facilitated photoswitching
1340 in live cells, where we performed a sequential acquisition, as Ex. 639 nm/ Em. 650/25 nm, Ex. 560
1341 nm/ Em. 575/30 nm, Ex. 405 nm/ Em. 488/40 nm. Further, a pulse of 30 iterations of excitation of
1342 405 nm was given. Then, the next cycle was Ex. 639 nm/ Em. 650/25 nm, Ex. 560 nm/ Em. 575/30
1343 nm. PSmOrange-C1-EPHA2 was given a 488 nm iteration instaed of 405 in one experiment as a
1344 positive control for photoswitching. (B) FRET Facilitated photoswitching images of PSmOrange-
1345 C1 and mT-Sapphire-C1 empty vectors, which served as a negative control. (C) FRET Facilitated
1346 photoswitching images of PSmOrange-C1-EPHA2 and mT-Sapphire-C1-Ephrin-B1.

1347 **S11 Fig. ELDA for *cis*-interaction.**

1348 Table shows data for ELDA analysis of 1:1 mixture of single knock-down of EPHA2 and Ephrin-
1349 B1.

1350 **S12 Fig. Western blotting and IHC of xenografts.**

1351 (A) 1.2×10^6 RCB1015 wild-type or Ephrin-B1 knocked-down cells were injected subcutaneously
1352 on the flanks of the SCID mice. Tumors were collected after 28 days, and tumor tissue lysate was
1353 prepared and probed for the indicated molecules. (B) 1.2×10^6 RCB1017 wild-type or EPHA2
1354 knocked-down cells were injected subcutaneously on the flanks of the SCID mice. Tumors were
1355 collected after 34 days, and western blot was performed as described. (C) RCB1015 xenograft
1356 sections were stained for EPHA2, Ephrin-B, and ALDH1A1. (D-F) Bar plots represent mean
1357 intensity per field of EPHA2, Ephrin-B1 or ALDH1A1 in control and knock-down sections.
1358 Statistical analysis was done by an unpaired-two-tailed students t-test. *, ***, *** represents
1359 $p<0.05$, $p<0.001$ and $p<0.0001$, respectively.

1360 **S13 Fig. Clinical data analyses.**

1361 (A) Univariate analysis depicting distribution of the Ephrin-B1 (*EFNB1*), *EPHA2*, and *EPHB2*
1362 mRNA levels in OSCC specimens (N=31) compared to normal samples (N=26), data was
1363 downloaded from the Gene Expression Omnibus data portal. The GEO accession number of the
1364 dataset was GSE13601. (B) Hierarchical clustering heat map analysis with TCGA mRNA data set
1365 of HNSCC (N=515) to check expression of *EFNB1*, *EPHA2*, and *EPHB2*. Each vertical line in the
1366 map represents a single patient. (C) Correlation between EPHA2 and Ephrin B1 was checked in
1367 TCGA as well as GSE data set using Pearson's correlation analysis.

1368 **S1 Table. Differential expression of membrane proteins in sphere and monolayer.**

1369 **S2 Table. Differential expression of phosphopeptides in sphere and monolayer in replicate 1.**

1370 **S3 Table. Differential expression of phosphopeptides in sphere and monolayer in replicate 2.**

1371 **S4 Table. Differential expression of phosphoproteins in sphere and monolayer of replicate 1**

1372 **and 2.**

1373 **S5 Table. Differentially regulated pathways in spheres compared to monolayer from replicate**

1374 **1 and 2.**

1375 **S6 Table. Differentially regulated pathways implicated in self-renewal.**

1376 **S7 Table. Differentially regulated phosphoproteins of Eph/Ephrin signaling pathway.**

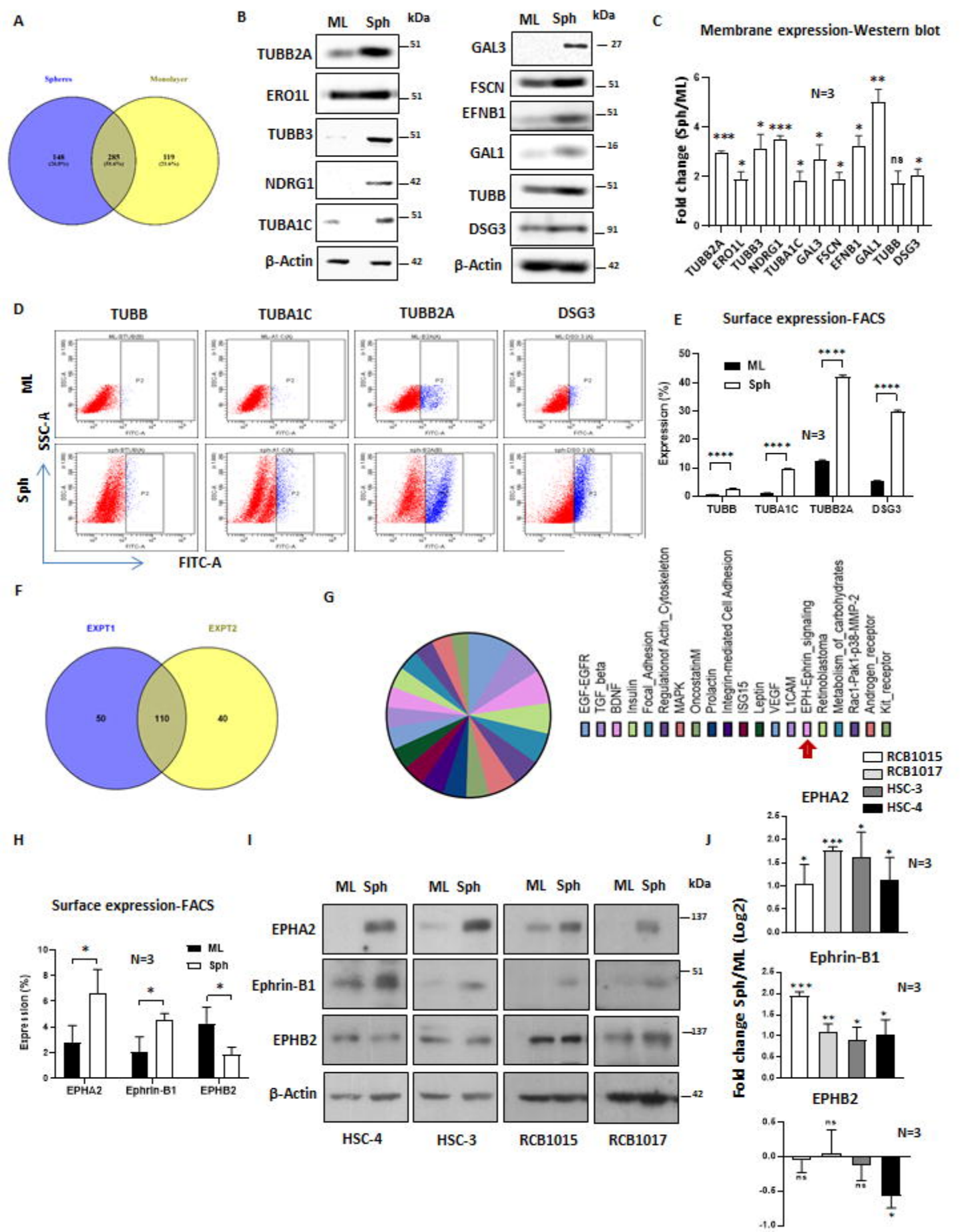
A
Spheres
Monolayer
B
ML Sph kDa
TUBB2A
ERO1L
TUBB3
NDRG1
TUBA1C
β-Actin
GAL3
FSCN
EFNB1
GAL1
TUBB
DSG3
β-Actin
C
Membrane expression-Western blot
Fold change (Sph/ML)
N=3
TUBB2A ERO1L TUBB3 NDRG1 TUBA1C GAL3 FSCN EFNB1 GAL1 TUBB DSG3
D
TUBB
TUBA1C
TUBB2A
DSG3
ML
Sph
SSC-A
FITC-A
E
Surface expression-FACS
ML
Sph
Expression (%)
N=3
TUBB TUBA1C TUBB2A DSG3
F
EXPT1
EXPT2
50
110
40
G
EGF-EGFR
TGF_beta
BDNF
Insulin
Focal_Adhesion
Regulationof Actin_Cytoskeleton
MAPK
Oncostatin M
Prolactin
Integrin-mediated Cell Adhesion
ISG15
Leptin
VEGF
L1CAM
EPH-Ephrin_signaling
Retinoblastoma
Metabolism_of_carbohydrates
Rac1-Pak1-p38-MMP-2
Androgen_receptor
Kit_receptor
RCB1015
RCB1017
HSC-3
HSC-4
EPHA2
Ephrin-B1
EPHB2
Fold change Sph/ML (Log2)
N=3
H
Surface expression-FACS
ML
Sph
Expression (%)
N=3
EPHA2 Ephrin-B1 EPHB2
I
ML Sph ML Sph ML Sph ML Sph kDa
EPHA2
Ephrin-B1
EPHB2
β-Actin
HSC-4 HSC-3 RCB1015 RCB1017
J

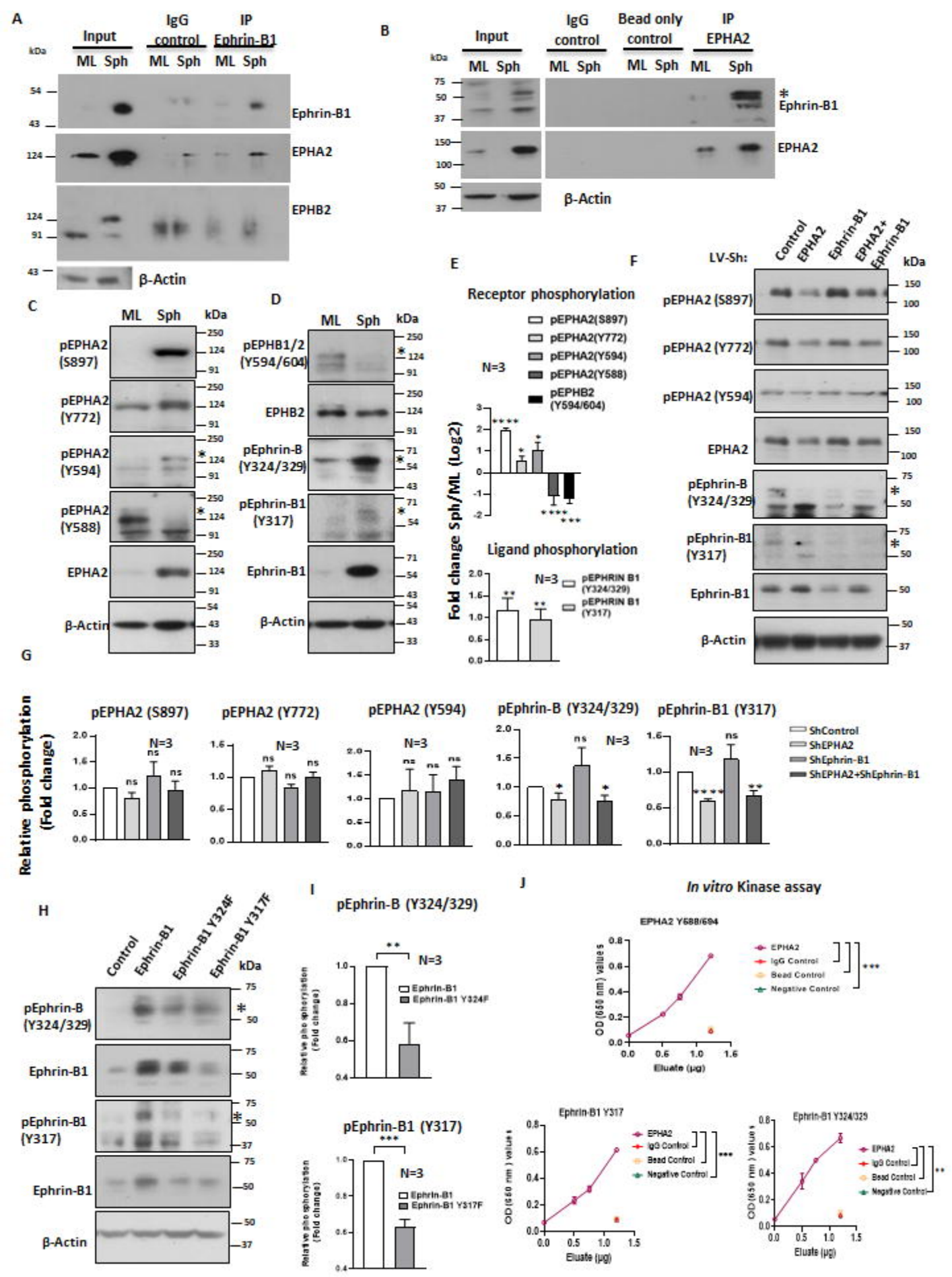
A
Input
IgG control
IP Ephrin-B1
ML Sph ML Sph ML Sph
kDa
Ephrin-B1
EPHA2
EPHB2
β-Actin
B
Input
IgG control
Bead only control
IP EPHA2
ML Sph ML Sph ML Sph ML Sph
Ephrin-B1
EPHA2
β-Actin
C
ML Sph kDa
pEPHA2 (S897)
pEPHA2 (Y772)
pEPHA2 (Y594)
pEPHA2 (Y588)
EPHA2
β-Actin
D
ML Sph kDa
pEPHB1/2 (Y594/604)
EPHB2
pEphrin-B (Y324/329)
pEphrin-B1 (Y317)
Ephrin-B1
β-Actin
E
Receptor phosphorylation
N=3
pEPHA2(S897)
pEPHA2(Y772)
pEPHA2(Y594)
pEPHA2(Y588)
pEPHB2 (Y594/604)
Fold change Sph/ML (Log2)
Ligand phosphorylation
N=3
pEPHRIN B1 (Y324/329)
pEPHRIN B1 (Y317)
F
LV-Sh: Control EPHA2 Ephrin-B1 EPHA2+ Ephrin-B1
kDa
pEPHA2 (S897)
pEPHA2 (Y772)
pEPHA2 (Y594)
EPHA2
pEphrin-B (Y324/329)
pEphrin-B1 (Y317)
Ephrin-B1
β-Actin
G
Relative phosphorylation (Fold change)
pEPHA2 (S897)
pEPHA2 (Y772)
pEPHA2 (Y594)
pEphrin-B (Y324/329)
pEphrin-B1 (Y317)
N=3
ns
ShControl
ShEPHA2
ShEphrin-B1
ShEPHA2+ShEphrin-B1
H
Control Ephrin-B1 Ephrin-B1 Y324F Ephrin-B1 Y317F
kDa
pEphrin-B (Y324/329)
Ephrin-B1
pEphrin-B1 (Y317)
Ephrin-B1
β-Actin
I
pEphrin-B (Y324/329)
N=3
Ephrin-B1
Ephrin-B1 Y324F
Relative phosphorylation (Fold change)
pEphrin-B1 (Y317)
Ephrin-B1
Ephrin-B1 Y317F
J
In vitro Kinase assay
EPHA2 Y688/694
EPHA2
IgG Control
Bead Control
Negative Control
OD (650 nm) values
Eluate (μg)
Ephrin-B1 Y317
Ephrin-B1 Y324/329

A

EPHA2+pEphrin-B Y324/329

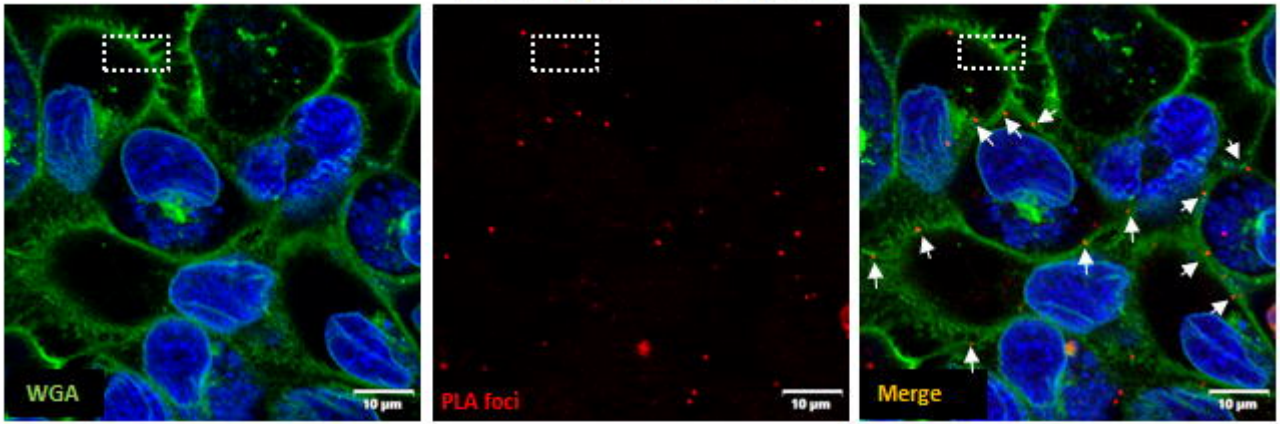

B

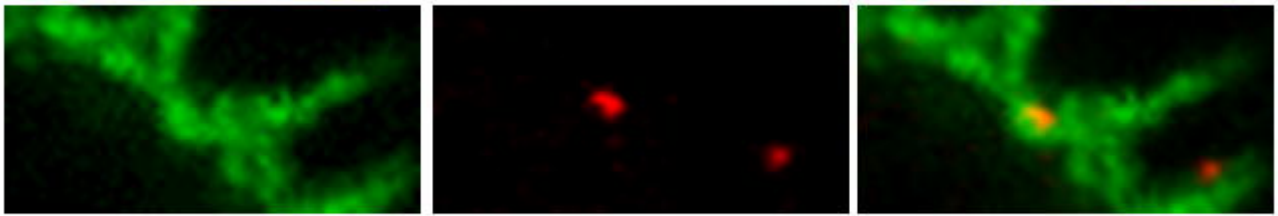

C

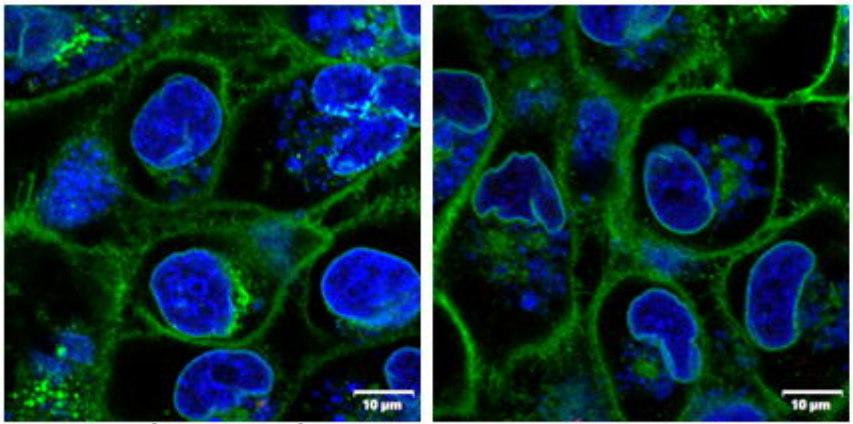

Secondary control

IgG control

D

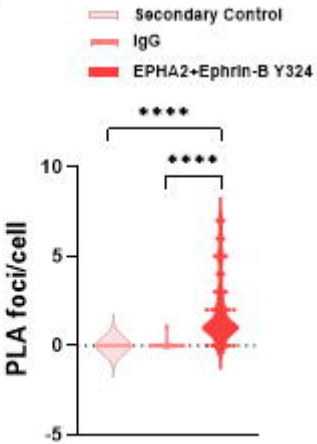

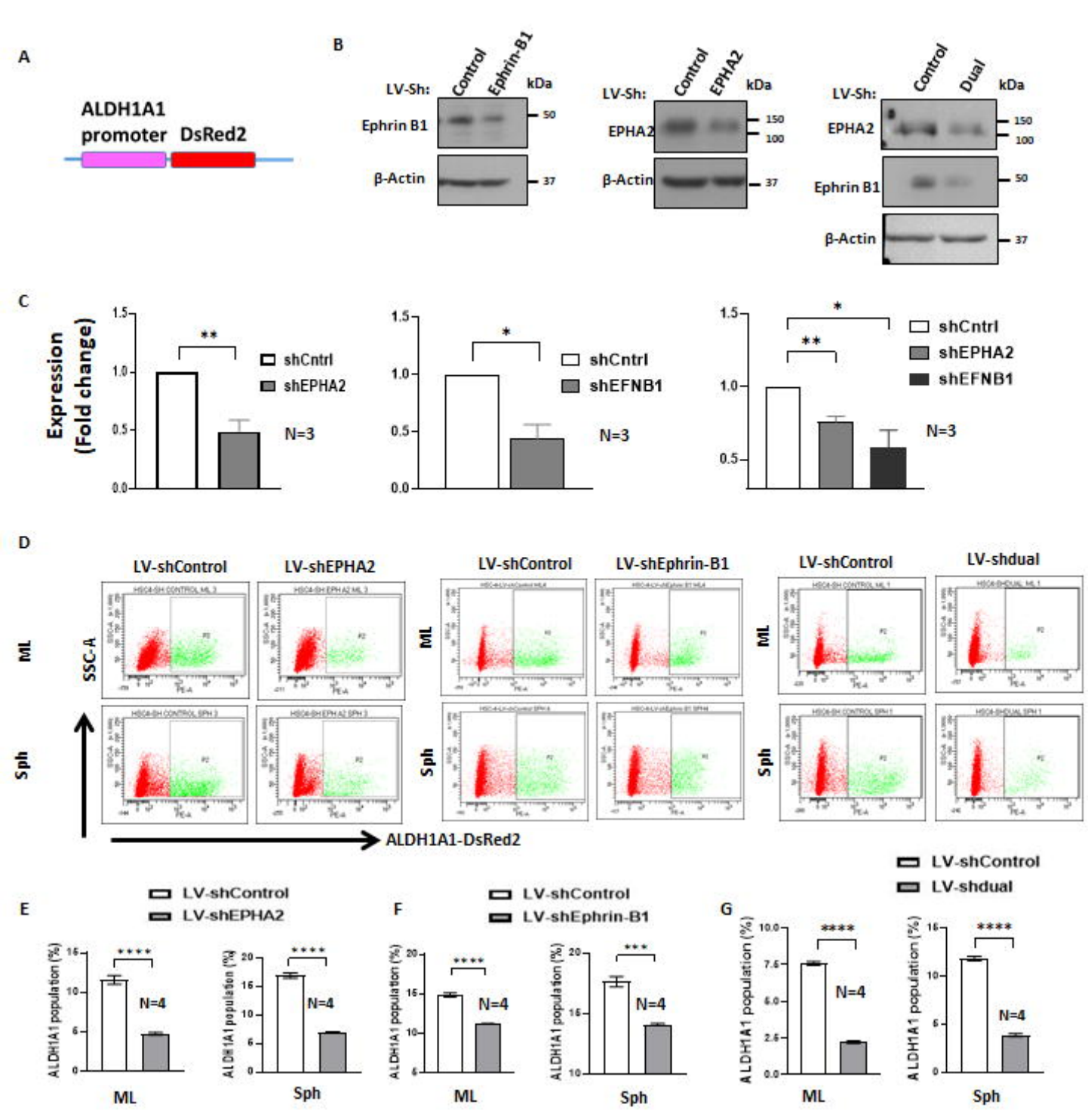
A
ALDH1A1
promoter
DsRed2
B
LV-Sh:
Control
Ephrin-B1
kDa
Ephrin B1
β-Actin
50
37
LV-Sh:
Control
EPHA2
kDa
EPHA2
β-Actin
150
100
37
LV-Sh:
Control
Dual
kDa
EPHA2
Ephrin B1
β-Actin
150
100
50
37
C
Expression
(Fold change)
shCntrl
shEPHA2
N=3
shCntrl
shEFNB1
N=3
shCntrl
shEPHA2
shEFNB1
N=3
D
LV-shControl
LV-shEPHA2
LV-shControl
LV-shEphrin-B1
LV-shControl
LV-shdual
ML
Sph
SSC-A
ALDH1A1-DsRed2
E
LV-shControl
LV-shEPHA2
ALDH1A1 population (%)
N=4
ML
Sph
F
LV-shControl
LV-shEphrin-B1
ALDH1A1 population (%)
N=4
ML
Sph
G
LV-shControl
LV-shdual
ALDH1A1 population (%)
N=4
ML
Sph

A

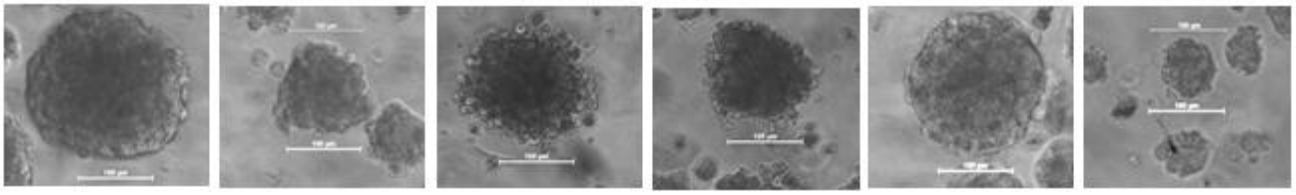

B

RCB1015	LV-sh	
	Control	EPHA2
Stem Cell frequency	1/694	1/3186
p-value	0.00000416	

RCB1015	LV-sh	
	Control	Ephrin-B1
Stem Cell frequency	1/2135	1/5545
p-value	0.000033	

RCB1015	LV-sh	
	Control	dual
Stem Cell frequency	1/1214	1/7378
p-value	$5.19*10^{-14}$	

C

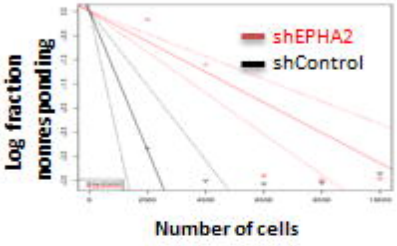

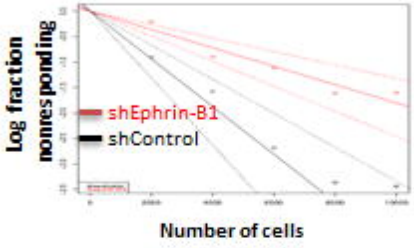

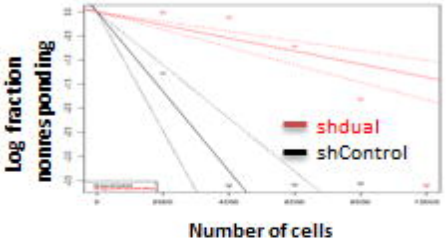

D

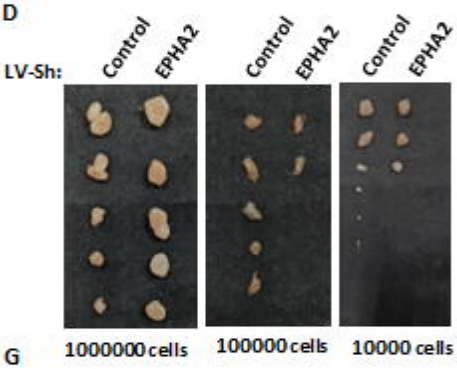

E

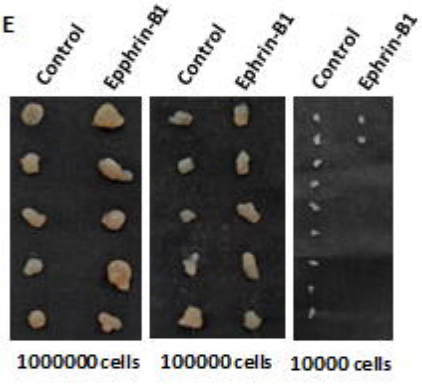

F

HSC-4	LV-sh	
	Control	EPHA2
Stem Cell frequency	1/180042	1/471201
p-value	0.0108	

RCB1015	LV-sh	
	Control	Ephrin-B1
Stem Cell frequency	1/4343	1/32574
p-value	0.00131	

G

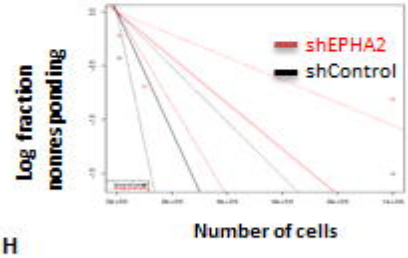

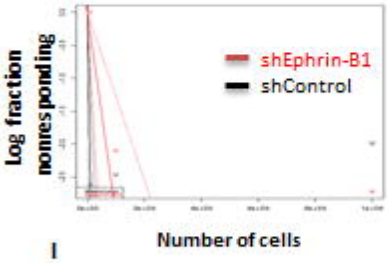

H

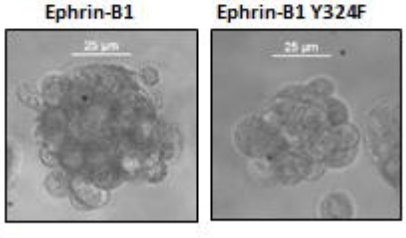

I

HSC-4	Over-expression	
	Ephrin-B1 RFP	Ephrin-B1 Y324F RFP
Stem Cell frequency	1/1332	1/2265
p- value	0.0562	

J

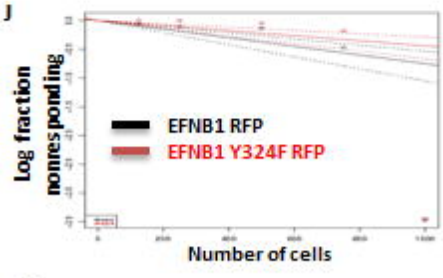

K

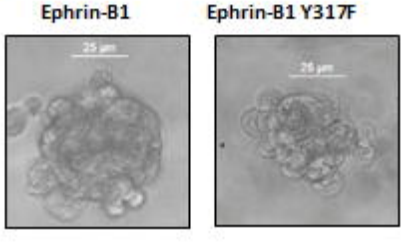

L

HSC-4	Over-expression	
	Ephrin-B1 RFP	Ephrin-B1 Y317F RFP
Stem Cell frequency	1/1377	1/2534
p-value	0.0459	

M

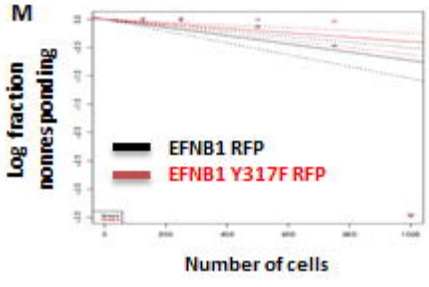

A

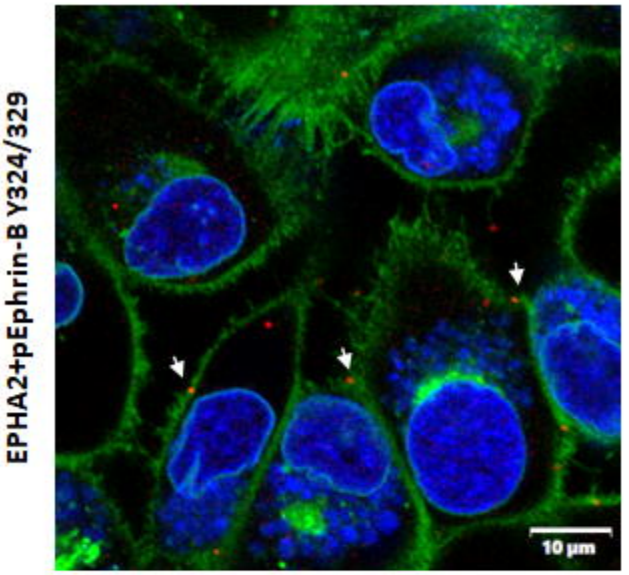

B

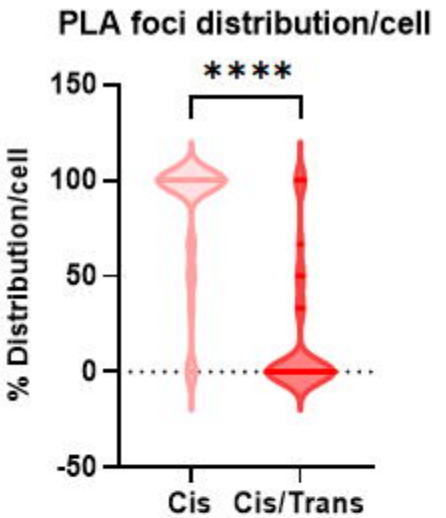

C

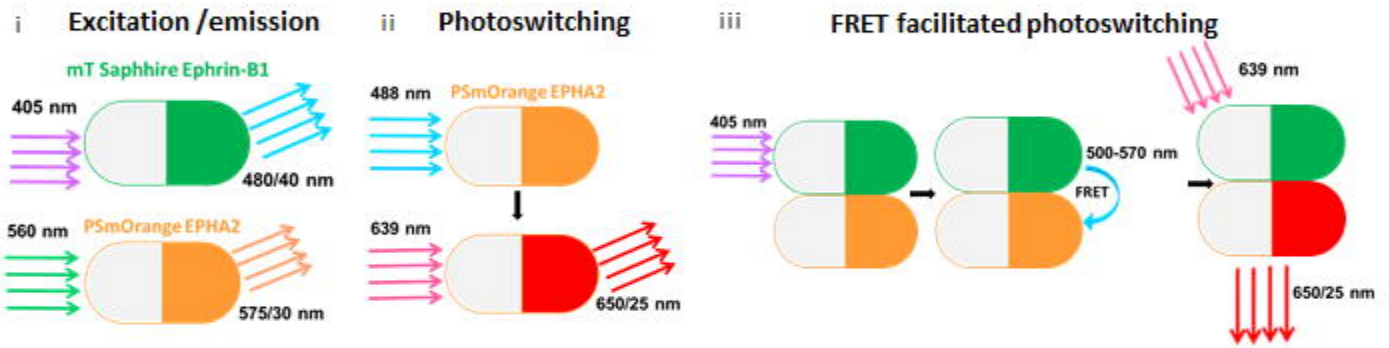

D

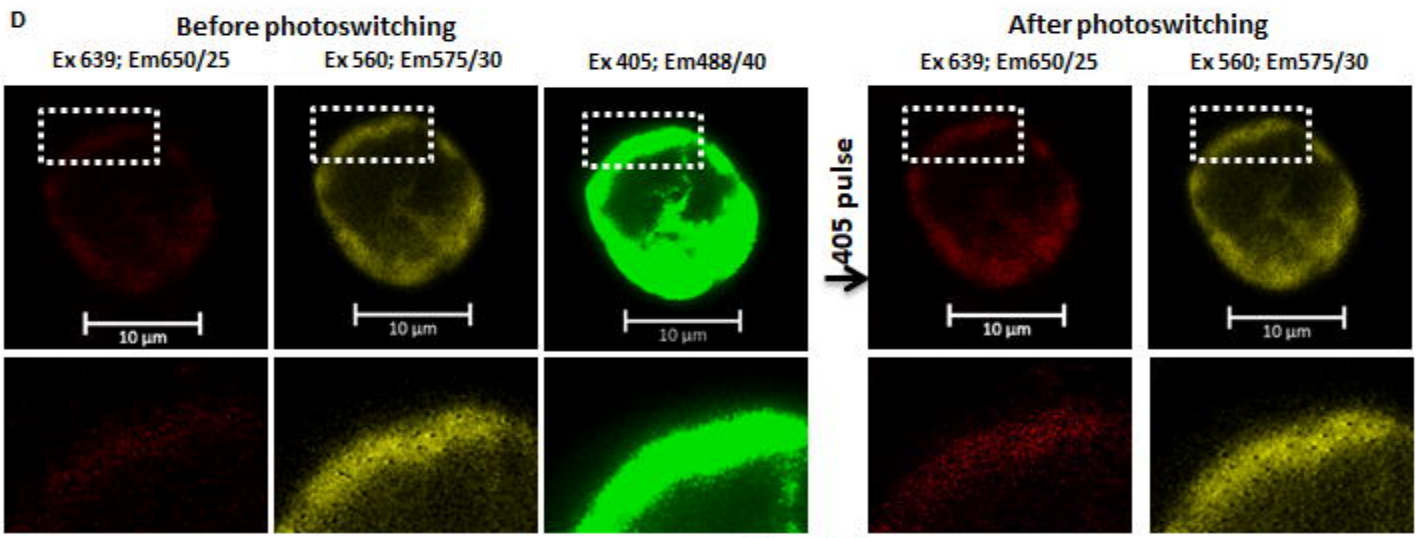

PSmOrange-EPHA2 + mT-Sapphire-Ephrin-B1

E

HSC-4	LV-sh	
	Control	EPHA2+ Ephrin-B1
Stem Cell frequency	1/251	1/582
p-value	0.00198	

F

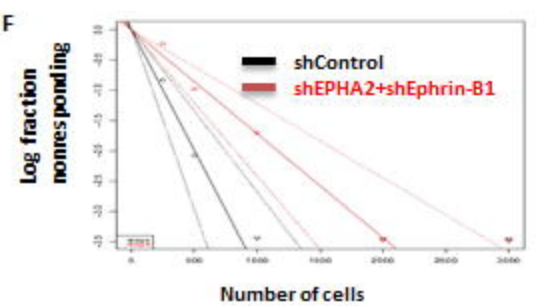

A

shControl
shEPHA2
shEphrin-B1
shControl
shdual

B

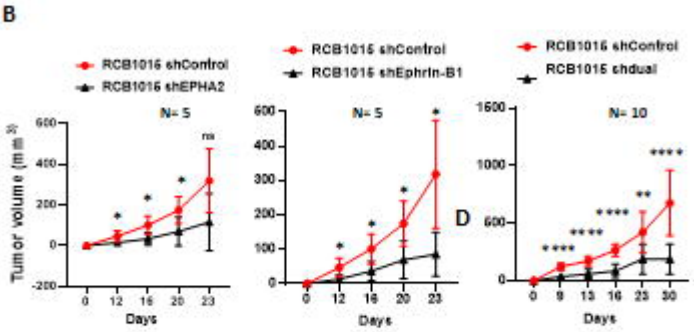
RCB1016 shControl
RCB1016 shEPHA2
N= 5
Tumor volume (mm³)
Days
RCB1016 shControl
RCB1016 shEphrin-B1
N= 5
Days
RCB1016 shControl
RCB1016 shdual
N= 10
Days

C

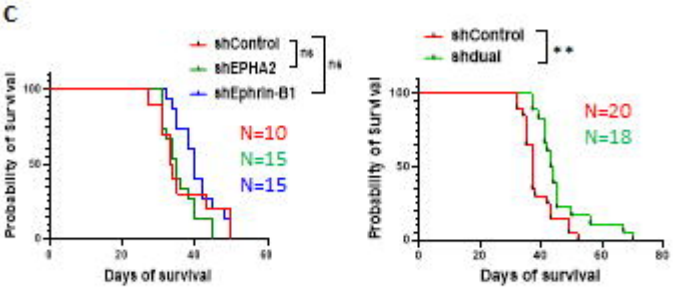
shControl
shEPHA2
shEphrin-B1
ns
ns
N=10
N=15
N=15
Probability of survival
Days of survival
shControl
shdual
**
N=20
N=18
Probability of survival
Days of survival

D

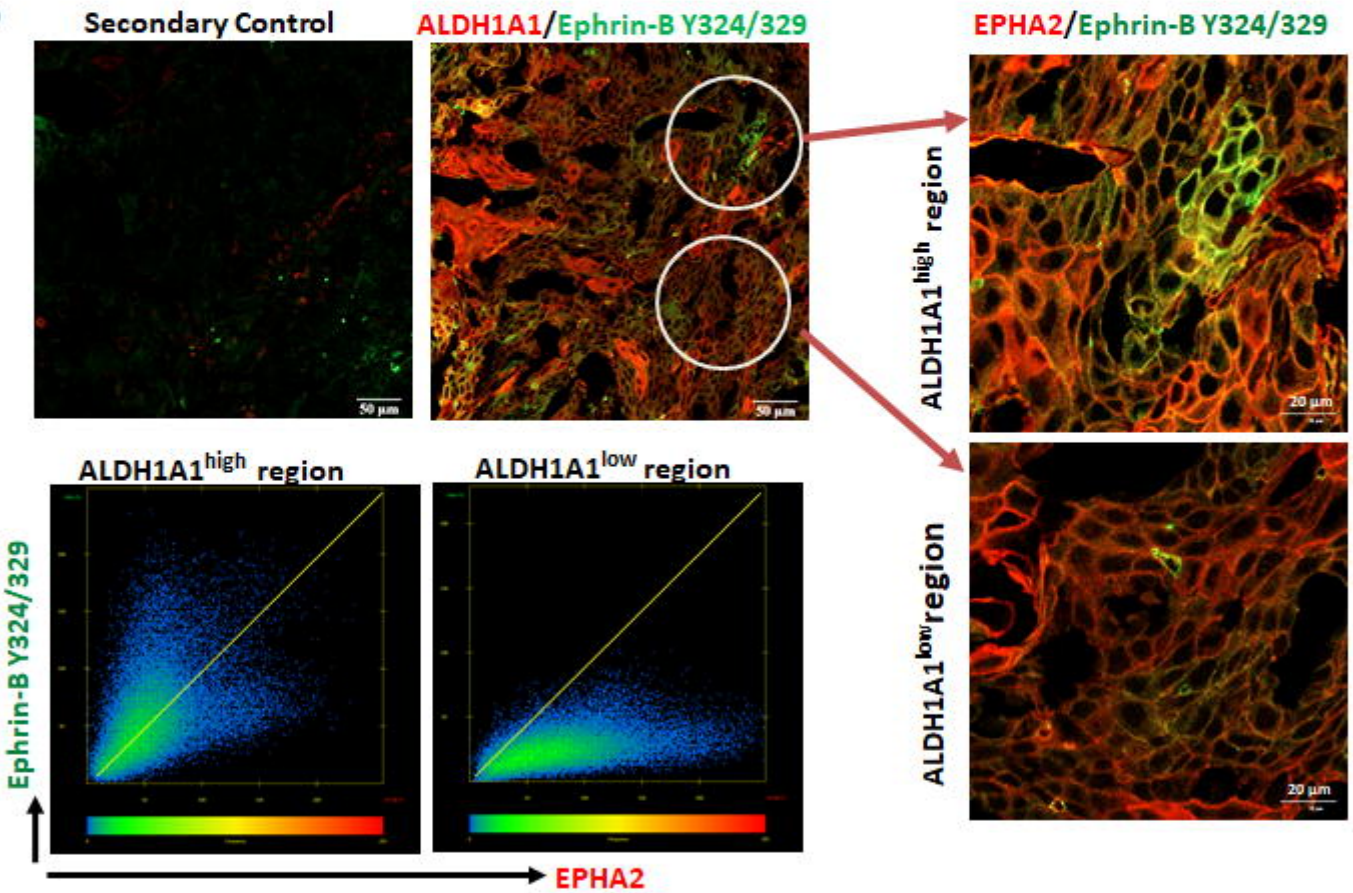
Secondary Control
ALDH1A1/Ephrin-B Y324/329
EPHA2/Ephrin-B Y324/329
50 µm
50 µm
ALDH1A1high region
20 µm
ALDH1A1low region
20 µm
ALDH1A1high region
ALDH1A1low region
Ephrin-B Y324/329
EPHA2

E

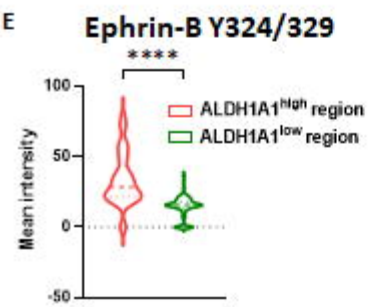
Ephrin-B Y324/329
****
Mean intensity
ALDH1A1high region
ALDH1A1low region

F

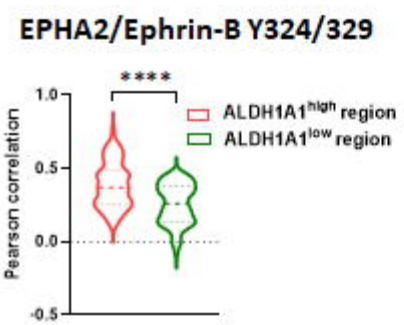
EPHA2/Ephrin-B Y324/329
****
Pearson correlation
ALDH1A1high region
ALDH1A1low region

A

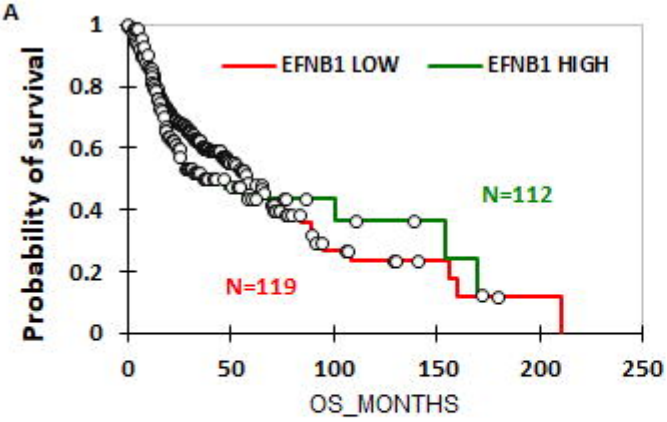

Test of equality of the survival distribution functions (DF = 1)

Statistic	Observed value	Critical value	p-value	alpha
Log-rank	0.011	3.841	0.916	0.050
Wilcoxon	0.029	3.841	0.866	0.050
Tarone-Ware	0.025	3.841	0.874	0.050

B

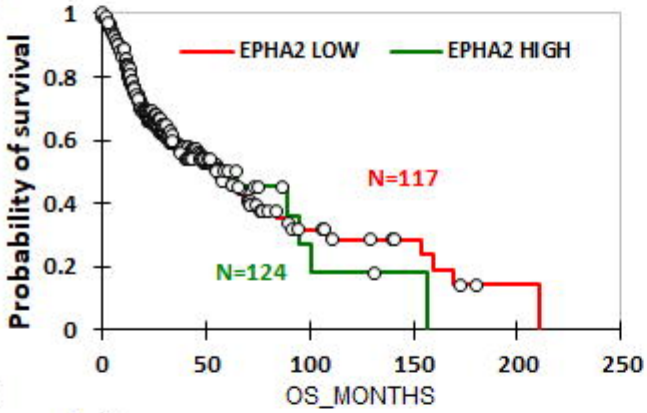

Test of equality of the survival distribution functions (DF = 1)

Statistic	Observed value	Critical value	p-value	alpha
Log-rank	0.285	3.841	0.593	0.050
Wilcoxon	0.001	3.841	0.978	0.050
Tarone-Ware	0.026	3.841	0.871	0.050

C

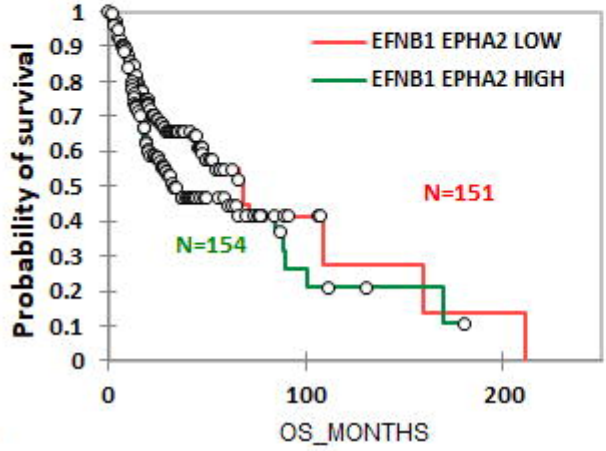

Test of equality of the survival distribution functions (DF=1)

Statistic	Observed value	Critical value	p-value	alpha
Log-rank	4.010	3.841	0.045	0.050
Wilcoxon	4.136	3.841	0.042	0.050
Tarone-Ware	4.426	3.841	0.035	0.050

D

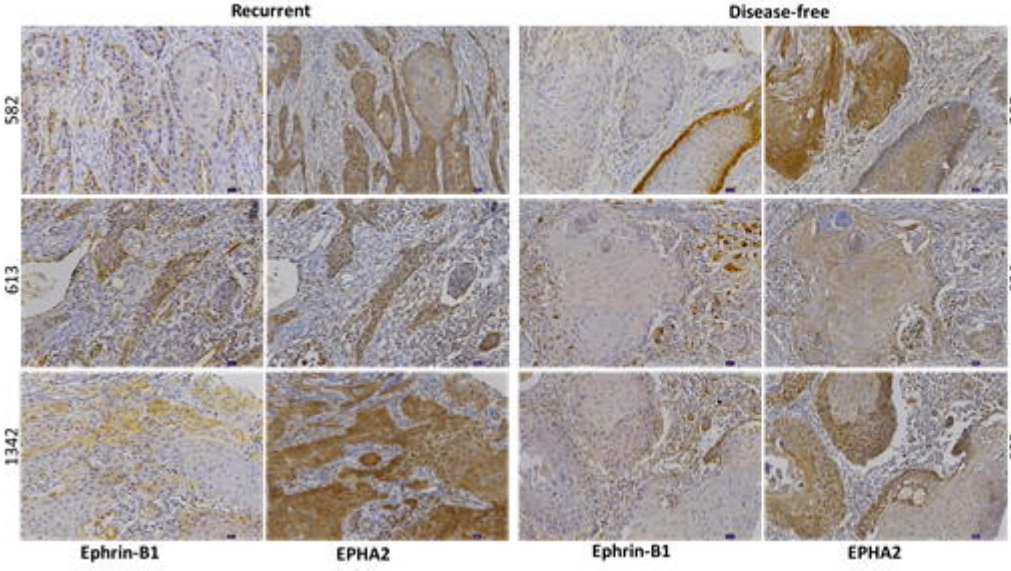
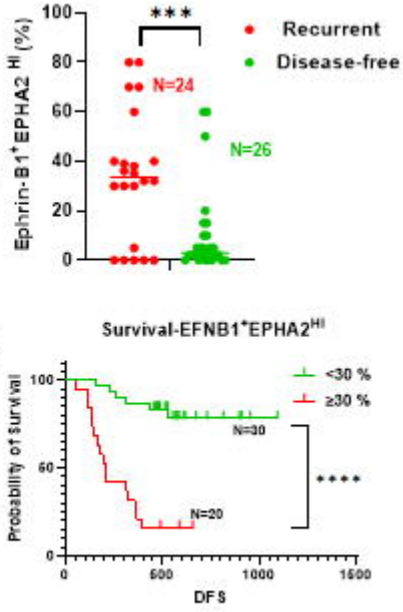
E